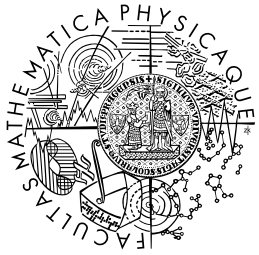

FACULTY
OF MATHEMATICS
AND PHYSICS
Charles University

BACHELOR THESIS

Adam Dvořák

Growth of the omega phase in metastable alloys: numerical simulations using phase-field method

Mathematical Institute of Charles University

Supervisor of the bachelor thesis: RNDr. Karel Tůma, Ph.D.
Study programme: Mathematical Modelling
Study branch: Mathematics

Prague 2024

I declare that I carried out this bachelor thesis independently, and only with the cited sources, literature and other professional sources. It has not been used to obtain another or the same degree.

I understand that my work relates to the rights and obligations under the Act No. 121/2000 Sb., the Copyright Act, as amended, in particular the fact that the Charles University has the right to conclude a license agreement on the use of this work as a school work pursuant to Section 60 subsection 1 of the Copyright Act.

In ..... date ....

Author's signature

I would like to thank my supervisor, RNDr. Karel Tůma, Ph.D., for his advice, patience and the time he spent with me on this thesis.

Název práce: Růst omega fáze v metastabilních slitinách: numerické simulace pomocí metody fázového pole

Autor: Adam Dvořák

Ústav: Matematický ústav Univerzity Karlovy

Vedoucí bakalářské práce: RNDr. Karel Tůma, Ph.D., Matematický ústav Univerzity Karlovy

Abstrakt: V mnoha metastabilních slitinách, jako jsou slitiny Ti a Zr-Nb, dochází k fázové transformaci z fáze β do metastabilní fáze ω. Fáze ω se převážně vytváří v materiálu během rychlého chlazení nebo izotermického stárnutí při zvýšených teplotách, nebo během deformace materiálu. Model fázového pole s různými bariérovými potenciály, jako jsou double well, double obstacle a Landau, je použitý k popisu těchto fázových transformací. Tato práce si klade za cíl porovnat vlastnosti těchto modelů. Pro všechny z nich odvozujeme několik semi-analytických výsledků, jako je energie a tvar rozhraní mezi fázemi β a ω, kritický poloměr zrníčka fáze ω pro jeho růst a rychlost šíření fáze ω. Ve druhé kapitole ověřujeme výsledky numericky pomocí kódu pro konečné elementy použitím Firedrake. V poslední části přizpůsobíme materiálové parametry tak, aby se předešlo kontaktu mezi různými variantami fáze ω.

Klíčová slova: metastabilní sloučeniny, $\beta \to \omega$ transformace, model fázového pole, numerická simulace, metoda konečných prvků

Title: Growth of the omega phase in metastable alloys: numerical simulations using phase-field method

Author: Adam Dvořák

Department: Mathematical Institute of Charles University

Supervisor: RNDr. Karel Tůma, Ph.D., Mathematical Institute of Charles University

Abstract: In many metastable alloys, such as Ti alloys and Zr-Nb alloys, phase transformation from β phase to the metastable ω phase occurs. The ω phase primarily forms in the material during rapid quenching or isothermal aging at elevated temperatures, or during material deformation. Phase-field model with different barrier potentials, such as the double well, double obstacle, and Landau, is used to describe these phase transformations. This work aims to compare the properties of these models. For all of them, we derive several semi-analytical results, such as the energy and shape of the interface between β and ω phases, the critical radius of ω phase grain for its growth, and the speed of ω phase propagation. In second chapter we verify the results numerically using the finite element code using Firedrake. In the last section, we appropriately adjust the material parameters to prevent contact between different variants of ω phase.

Keywords: metastable alloys, $\beta \to \omega$ transformation, phase-field model, numerical simulation, finite element method

Contents

Introduction

In recent years, dominant experimental research has focused on describing phase transformations in metastable alloys, which are responsible for a wide range of mechanical properties. The use of thermomechanical treatments has led to extensive utilization of metastable alloys in the aerospace industry and medicine. Better understanding of the formation and evolution of the ω phase may lead to recommendations for alloy design and processing. The ω phase in titanium alloys forms finely dispersed, submicron precipitates that are coherent with the parent β phase, for details see [1]. There are three main conditions under which the ω phase forms:

- When the β stabilizer content is high enough, the athermal ω phase forms during rapid quenching, which is a displacive and diffusionless process.
- The ω phase can also be formed during isothermal aging in the temperature range of approximately 100–500 °C.
- Deformation at room temperature can also cause the formation or increase in the amount of the ω phase in some types of metastable alloys.

Despite being energetically favorable, it is not observed experimentally that the ω phase completely fills the entire volume of the body. From a crystallographic perspective, the ω phase can have either hexagonal or trigonal symmetry. The morphology of the ω phase can be either ellipsoidal or cuboidal and depends on the misfit of lattice parameters between the ω and β phases.

The occurrence of ω phase has a significant impact on the mechanical properties of metastable alloys. The precipitation of metastable ω particles leads to an increase in yield strength, a reduction in ductility of the alloy, and induces material embrittlement, which can lead to product failure. Hence, one of the objectives is to curb its propagation. For a better understanding of the formation and evolution of the ω phase in titanium alloys, the phase-field modeling method appears to be suitable. The phase-field method allows modeling various problems in microstructure evolution, including solid-state phase transformations. Developing a specialized phase-field model for the β to ω transformation will enable us to resolve long-debated mechanisms of ω phase formation. Compared to more fundamental approaches, such as molecular dynamics (MD) and *ab initio* methods, the phase-field approach allows modeling at larger scales and captures details of the evolving microstructure.

In the phase-field method, individual phases are described by global unknowns called phase field variables. These variables can be interpreted as phase volume fractions, and they are individually bounded between 0 and 1. In the corresponding phase, the phase field variable is equal to one, while in the other phases, it is zero. Phase field variables can be used for direct interpolation of various material properties within diffuse interfaces. The evolution of these variables is governed by partial differential equations and often leads to a variational problem, where the entire evolutionary process is formulated within the framework of incremental energy minimization. The main advantage is the continuous parameter change across phase interfaces, making the interfaces diffuse. Due to the diffuse nature

of the β/ω interfaces, the phase-field method is suitable for modeling ω phase formation.

The aim of this work is to compare the qualitative properties of existing models - the double obstacle, double well, and Landau models - that were adopted for these phase transitions. In the first chapter, we describe the energies involved in phase transformation, then we describe these models and formulate their evolution through functional minimization. Based on this interpretation, we derive theoretical properties of all mentioned models such as the thickness, shape, and energy of the interface between β and ω phases, and the minimum size of omega phase grains for its growth. For the Landau model and double-obstacle model, we derive the speed of their interface propagation. In the second chapter, we focus primarily on numerically verifying the derived properties in Firedrake using finite element method. Finally, we appropriately adjust the material parameters to prevent contact between different variants of ω.

1. Models

1.1 Problem description

In Titanium alloys occur phase transitions from the β to ω phase. The ω phase is preferred in alloys because it has lower phase energy. Thus leading to its propagation. In this alloys, the β and ω phases mainly form with crystal structures of body-centered cubic (bcc) and trigonal or hexagonal, respectively. Therefore, the β phase is a more symmetric phase, and its transformation yields multiple types of ω, as described below.

The evolution of phases in the alloy is governed by an equation that minimizes the total body energy Ψ, which is the volume integral of the energy density ψ

$$\Psi = \int_\Omega \psi \, dV. \tag{1.1}$$

Energy density can be divided into four types: energy of phase ψ_{phas}, potential barrier between phases ψ_{bar}, gradient energy ψ_{grad}, and elastic energy ψ_{el}

$$\psi = \psi_{phas} + \psi_{bar} + \psi_{grad} + \psi_{el}. \tag{1.2}$$

The first type is the phase energy, which represents the energy difference between the parent phase β and the energy induced by the presence of ω phases. We denote the energy difference between the parent phase β and the energy of the given phase ω_i as ϕ_i.

The second type of energy is the potential barrier between individual phases, which is the necessary energy for phase change. Examples include double obstacle or double well potential, which is discussed in the sections below.

The third type of energy is the gradient energy, which typically depends on the partial derivatives of the phase field variable η_i. It therefore appears together with the potential energy barrier at the phase interfaces.

Elastic energy is caused by changes in microstructure. Different deformation tensors of individual phases result in stress within the material, which is a source of the elastic energy.

The entire algebraic part of the energy density (i.e. the part not containing gradients), represented as the sum of ψ_{bar} and ψ_{phas}, we denote as ψ_{chem} and referred to as chemical energy

$$\psi_{chem} = \psi_{bar} + \psi_{phas}. \tag{1.3}$$

The part of energy density occurring at the phase interface, called interface energy, is denoted as ψ_{int} and has the following form

$$\psi_{int} = \psi_{bar} + \psi_{grad}. \tag{1.4}$$

We denote their total values in the body as Ψ with the corresponding subscript, for example

$$\Psi_{int} = \int_\Omega \psi_{int} \, dV \tag{1.5}$$

denotes total interface energy.

1.2 Basic of continuum mechanic and β to ω transformaion

1.2.1 Continuum mechanics

Let us have $\Omega \subset \mathbb{R}^3$ as a reference configuration. For each $\mathrm{X} \in \Omega$, there exists a mapping $\chi : \Omega \to \chi(\Omega)$ such that any deformation can be described by this function as $\chi(\mathrm{X}) = \boldsymbol{x}$. $\chi(\Omega) \subset \mathbb{R}^3$ is called current configuration and $\boldsymbol{x}$ represents the point in current configuration.

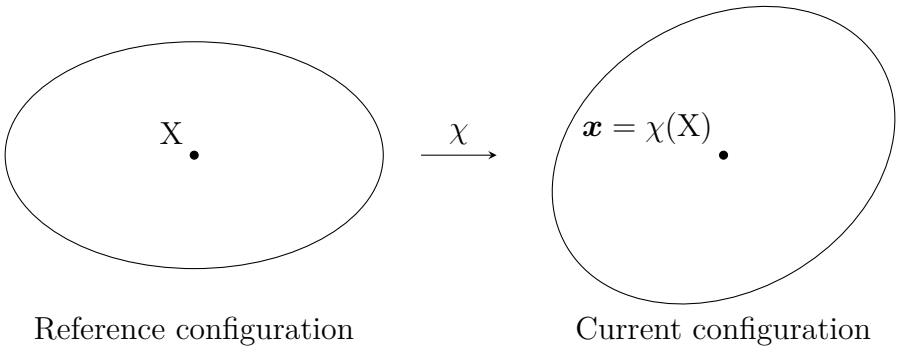

Figure 1.1: The deformation χ acting on Ω.

Let us define kinematic quantities to describe our material

- $\mathbb{F}$ – the deformation tensor as a matrix with the components

$$(\mathbb{F})_{ij} = \frac{\partial \chi_i(\mathrm{X})}{\partial \mathrm{X}_j}, \quad i, j = 1, 2, 3. \tag{1.6}$$

- $\boldsymbol{u}(\mathrm{X}) = \chi(\mathrm{X}) - \mathrm{X}$ – the displacement. We can regard the deformation gradient as a sum $\mathbb{F} = \nabla \boldsymbol{u} + \mathbb{I}$, it follows from:

$$\frac{\partial \boldsymbol{u}_i(\mathrm{X})}{\partial \mathrm{X}_j} = \frac{\partial \chi_i(\mathrm{X})}{\partial \mathrm{X}_j} - \mathbb{I}_{ij}. \tag{1.7}$$

- $\mathbb{E} = \frac{1}{2}(\mathbb{F}^T\mathbb{F} - \mathbb{I})$ – the Green strain tensor. Using identity $\mathbb{F} = \nabla \boldsymbol{u} + \mathbb{I}$, we obtain:

$$\mathbb{E} = \frac{1}{2}((\nabla \boldsymbol{u} + \mathbb{I})^T(\nabla \boldsymbol{u} + \mathbb{I}) - \mathbb{I}) = \frac{1}{2}(\nabla \boldsymbol{u} + (\nabla \boldsymbol{u})^T + (\nabla \boldsymbol{u})(\nabla \boldsymbol{u})^T) \tag{1.8}$$

- $\mathbb{T}$ – the Cauchy stress tensor. Expressing the traction acting on the deformed surface in the current configuration $\mathbb{T}(\boldsymbol{x})\boldsymbol{n}$, where $\boldsymbol{n}$ is the normal to the surface.

- $\mathbb{P} = (\mathrm{det}\mathbb{F})\mathbb{T}\mathbb{F}^{-T}$ – the first Piola-Kirchhoff stress tensor. Expressing $\mathbb{T}(\boldsymbol{x})\boldsymbol{n}$ in the reference configuration. For a hyperelastic material it can be computed from elastic energy density function ψ_{el} as

$$\mathbb{P} = \frac{\partial \psi_{el}}{\partial \mathbb{F}}. \tag{1.9}$$

  We can also compute it as $\mathbb{P} = \frac{\partial \psi_{el}}{\partial \nabla \boldsymbol{u}}$, using the identity above.

We recall the balance equation in reference configuration

$$\begin{aligned} \rho \det \mathbb{F} &= \rho_R, && \text{balance of mass,} \\ \rho_R \frac{\partial^2 \chi(\mathrm{X}, t)}{\partial t^2} &= \mathrm{Div}_{\mathrm{X}} \mathbb{P} + \rho_R \mathbf{f}, && \text{balance of linear momentum,} \end{aligned}$$

where ρ_R is the density in the reference configuration, ρ is the density in the current configuration and $\mathbf{f}$ represents the external forces. In this model we consider only the quasi-static situation so the second time derivative in the balance of linear momentum disappears. We also neglect external force $\mathbf{f} = 0$. Thus we obtain our local displacement $\boldsymbol{u}$ by solving the mechanical equilibrium condition

$$\mathrm{Div}_{\mathrm{X}} \mathbb{P} = 0. \tag{1.10}$$

In the rest of the thesis we consider only small deformation, thus $|\nabla \boldsymbol{u}| \ll 1$. Then, for simplicity, we can take $\rho = \rho_R = const.$ and the first Piola-Kirchhoff stress tensor $\mathbb{P}$ and Cauchy stress tensor $\mathbb{T}$ coincide and we denote them by σ and in isotropic material can be expressed as

$$\sigma = \frac{E}{1+\nu} \left[\epsilon + \frac{\nu}{1-2\nu} \mathrm{tr}(\epsilon) \mathbb{I} \right], \tag{1.11}$$

where E is Young's modulus of elasticity, ν is the Poisson ratio and ϵ is tensor of small deformations

$$\epsilon = \frac{1}{2} \left(\nabla \boldsymbol{u} + (\nabla \boldsymbol{u})^T \right). \tag{1.12}$$

The strain-energy density function for the isotropic small strain elasticity model is

$$\psi_{el} = \frac{E}{2(1+\nu)} \left[|\epsilon|^2 + \frac{\nu}{1-2\nu} \mathrm{tr}^2(\epsilon) \right]. \tag{1.13}$$

1.2.2 Transformation β to ω

In this subsection, we follow the book by Bhattacharya [2]. We define a Bravaris lattice $L(\mathbf{a}_i, \mathbf{o})$ as an infinite set of points in space generated by a set of linearly independent vectors $\{\mathbf{a}_1, \mathbf{a}_2, \mathbf{a}_3\}$ as

$$L(\mathbf{a}_1, \mathbf{a}_2, \mathbf{a}_3) = \left\{ \mathbf{x} : \mathbf{x} = \sum_{i=1}^{3} \nu_i \mathbf{a}_i \text{ where } \nu_i \in \mathbb{N}, \text{for i = 1, 2, 3} \right\},$$

and its point group $\mathcal{P}$ as a finite set of rotations $\mathbf{R}$ that map a Bravaris lattice back to itself:

$$\mathcal{P} = \{ \mathbf{R} : L(\mathbf{a}_1, \mathbf{a}_2, \mathbf{a}_3) = L(\mathbf{R}\mathbf{a}_1, \mathbf{R}\mathbf{a}_2, \mathbf{R}\mathbf{a}_3), \mathbf{R} \text{ is rotation matrix} \}.$$

$|\mathcal{P}|$ is the number of rotations. The β phase has a body-centered cubic (bcc) structure and number of their rotations is $|\mathcal{P}_\beta| = 24$ for β. The point group of β phase contains the following rotations

$$\begin{array}{ccc} \mathbf{R}(\boldsymbol{e}_1, \frac{\pi}{2}) & \mathbf{R}(\boldsymbol{e}_1, \pi) & \mathbf{R}(\boldsymbol{e}_1, \frac{3\pi}{2}) \\ \mathbf{R}(\boldsymbol{e}_2, \frac{\pi}{2}) & \mathbf{R}(\boldsymbol{e}_2, \pi) & \mathbf{R}(\boldsymbol{e}_2, \frac{3\pi}{2}) \\ \mathbf{R}(\boldsymbol{e}_3, \frac{\pi}{2}) & \mathbf{R}(\boldsymbol{e}_3, \pi) & \mathbf{R}(\boldsymbol{e}_3, \frac{3\pi}{2}) \\ \mathbf{R}(\frac{1}{\sqrt{2}}(\boldsymbol{e}_1 + \boldsymbol{e}_2), \pi) & \mathbf{R}(\frac{1}{\sqrt{2}}(\boldsymbol{e}_2 + \boldsymbol{e}_3), \pi) & \mathbf{R}(\frac{1}{\sqrt{2}}(\boldsymbol{e}_3 + \boldsymbol{e}_1), \pi) \\ \mathbf{R}(\frac{1}{\sqrt{2}}(\boldsymbol{e}_1 - \boldsymbol{e}_2), \pi) & \mathbf{R}(\frac{1}{\sqrt{2}}(\boldsymbol{e}_2 - \boldsymbol{e}_3), \pi) & \mathbf{R}(\frac{1}{\sqrt{2}}(\boldsymbol{e}_3 - \boldsymbol{e}_1), \pi) \end{array}$$

$$\begin{array}{ll}\mathbf{R}(\frac{1}{\sqrt{3}}(\boldsymbol{e}_1+\boldsymbol{e}_2+\boldsymbol{e}_3),\frac{2\pi}{3}) & \mathbf{R}(\frac{1}{\sqrt{3}}(\boldsymbol{e}_1+\boldsymbol{e}_2-\boldsymbol{e}_3),\frac{2\pi}{3})\\ \mathbf{R}(\frac{1}{\sqrt{3}}(\boldsymbol{e}_1-\boldsymbol{e}_2+\boldsymbol{e}_3),\frac{2\pi}{3}) & \mathbf{R}(\frac{1}{\sqrt{3}}(-\boldsymbol{e}_1+\boldsymbol{e}_2+\boldsymbol{e}_3),\frac{2\pi}{3})\\ \mathbf{R}(\frac{1}{\sqrt{3}}(\boldsymbol{e}_1+\boldsymbol{e}_2+\boldsymbol{e}_3),\frac{4\pi}{3}) & \mathbf{R}(\frac{1}{\sqrt{3}}(\boldsymbol{e}_1-\boldsymbol{e}_2+\boldsymbol{e}_3),\frac{4\pi}{3})\\ \mathbf{R}(\frac{1}{\sqrt{3}}(\boldsymbol{e}_1-\boldsymbol{e}_2+\boldsymbol{e}_3),\frac{4\pi}{3}) & \mathbf{R}(\frac{1}{\sqrt{3}}(-\boldsymbol{e}_1+\boldsymbol{e}_2+\boldsymbol{e}_3),\frac{4\pi}{3})\end{array}$$

I.

Where $\boldsymbol{e}_i$, $i=1,2,3$ are the basis vectors. If we apply all rotations $\mathbf{R}^T\mathbf{U}_1^t\mathbf{R}$ on the firs bain strain tensor $\mathbf{U}_1^t$ of ω

$$\mathbf{U}_1^t=\begin{pmatrix}\epsilon_1 & \epsilon_2 & \epsilon_2\\ \epsilon_2 & \epsilon_1 & \epsilon_2\\ \epsilon_2 & \epsilon_2 & \epsilon_1\end{pmatrix}, \tag{1.14}$$

we obtain only three additional bain strain tensors, thus we have

$$\mathbf{U}_1^t=\begin{pmatrix}\epsilon_1 & \epsilon_2 & \epsilon_2\\ \epsilon_2 & \epsilon_1 & \epsilon_2\\ \epsilon_2 & \epsilon_2 & \epsilon_1\end{pmatrix}, \qquad \mathbf{U}_2^t=\begin{pmatrix}\epsilon_1 & -\epsilon_2 & -\epsilon_2\\ -\epsilon_2 & \epsilon_1 & \epsilon_2\\ -\epsilon_2 & \epsilon_2 & \epsilon_1\end{pmatrix},$$
$$\mathbf{U}_3^t=\begin{pmatrix}\epsilon_1 & -\epsilon_2 & \epsilon_2\\ -\epsilon_2 & \epsilon_1 & -\epsilon_2\\ \epsilon_2 & -\epsilon_2 & \epsilon_1\end{pmatrix}, \qquad \mathbf{U}_4^t=\begin{pmatrix}\epsilon_1 & \epsilon_2 & -\epsilon_2\\ \epsilon_2 & \epsilon_1 & -\epsilon_2\\ -\epsilon_2 & -\epsilon_2 & \epsilon_1\end{pmatrix},$$

where $\epsilon_1=v+\frac{1}{3}u$, $\epsilon_2=\frac{1}{3}u$, $v=a_\omega/(\sqrt{2}a_\beta)-1$ and $u=2c_\omega/(\sqrt{3}a_\beta)-a_\omega(\sqrt{2}a_\beta)$. a_β, a_ω, and c_ω are lattice constants of β and ω phases, respectively. The first bain strain tensor $\mathbf{U}_1^t$ can be derived from geometry of cubic and trigonal Bravaris lattice, see [3]. Therefore, there are four types of ω. The number N of all variants of ω can generally be calculated as the ratio of the number of rotations in the point group

$$N=\frac{|\mathcal{P}_\beta|}{|\mathcal{P}_\omega|}. \tag{1.15}$$

1.3 Models for one ω phase

The energy density ψ of the system undergoing an athermal phase transformation comprises following components: phase, barrier, gradient and elastic energy density

$$\psi=\psi_{phase}+\psi_{bar}+\psi_{grad}+\psi_{el}. \tag{1.16}$$

Their volume integral over the investigated domain Ω is equal to Ψ

$$\Psi=\int_\Omega(\psi_{phase}+\psi_{bar}+\psi_{grad}+\psi_{el})\,dV. \tag{1.17}$$

In the following, for all models, we describe all these energies for a single ω variant, except for elastic energy. In this case we have only one phase-field variable η. The phase field variable η is a scalar function defined over Ω, and its values represent volume fractions between the β and ω phases.

1.3.1 Double well

The double well model combines the barrier energy ψ_{bar} between phases and the gradient energy ψ_{grad}, which is referred to as the interface energy

$$\psi_{int} = \psi_{bar} + \psi_{grad}. \tag{1.18}$$

The barrier energy is given by double well potential

$$\psi_{bar} = \frac{6\gamma}{\ell}\eta^2(1-\eta)^2. \tag{1.19}$$

If $\eta = 0$ it means that there is only parent phase β and if $\eta = 1$ there is only ω phase. An advantage of this model is that this potential maintained the values of η between zero and one, where it reaches its minimum, see Fig. 1.2. interface energy between β and ω phase is defined as

$$\psi_{int} = \gamma\left(\frac{3\ell}{2}|\nabla\eta|^2 + \frac{6}{\ell}\eta^2(1-\eta)^2\right), \tag{1.20}$$

where the constants γ and ℓ determine interface energy per unit area and the thickness of interface, respectively.

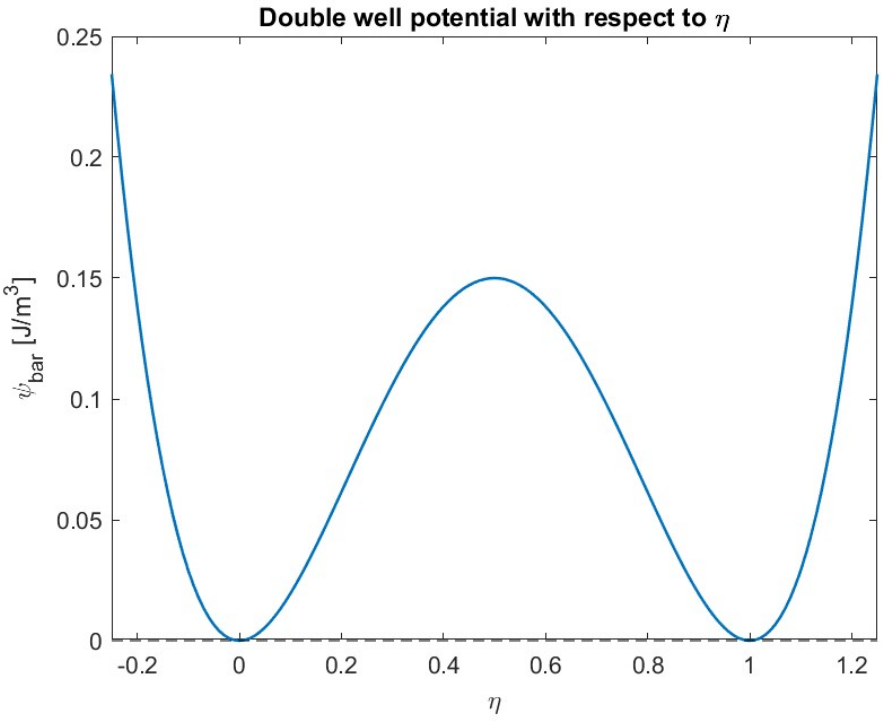

Figure 1.2: Double well potential ψ_{bar} as a function of the phase field variable η. We set the constant $\ell = 0.5$ nm, $\gamma = 0.2$ J/m^2

The phase energy ψ_{phas} is defined as the volume fraction of the β and ω phase η multiplied by the difference in energy between the parent phase β and ω phase, referred to as ϕ

$$\psi_{phas} = \eta\phi. \tag{1.21}$$

Unlike the Landau model described below, this phase energy mixing is linear.

1.3.2 Double obstacle

In the double obstacle model, we use the double obstacle potential as the barrier energy. For one ω phase the potential barrier ψ_{bar} is given by

$$\psi_{bar} = \frac{4\gamma}{\pi\ell}\eta(1-\eta), \tag{1.22}$$

where ℓ determine the thickness of the interface and γ is the interface energy per unit area. The sum of the potential barrier energy and the gradient energy, as well as in the double well model, yields the interface energy

$$\psi_{int} = \psi_{bar} + \psi_{grad}, \tag{1.23}$$

with the following form

$$\tilde{\psi}_{int} = \gamma\left(\frac{4\ell}{\pi}|\nabla\eta|^2 + \frac{4}{\pi\ell}\eta(1-\eta)\right). \tag{1.24}$$

This energy is suitable for studying interfaces, and by simple calculation, we obtain its shape, energy per unit area, and the thickness. Unfortunately, this potential does not have a minimum at $\eta = 0$ or $\eta = 1$, see Fig. 1.3 so we have to put some restriction on phase field variable η such as penalization for a single ω phase if η is outside of interval $[0, 1]$. In order to keep phase field variable in interval $[0, 1]$ we need to define a penalty $P(\eta)$ in case the parameter is not in the desired interval

$$P(\eta) = \begin{cases} \frac{1}{2}c\eta^2 & \eta < 0, \\ 0 & \eta \in [0,1], \\ \frac{1}{2}c(1-\eta)^2 & \eta > 1. \end{cases} \tag{1.25}$$

where c is a big constant, e.g. c = 1000, see Fig. 1.4. This function is added to $\tilde{\psi}_{int}$, i.e. $\psi_{int} = \tilde{\psi}_{int} + P(\eta)$. The phase energy ψ_{phas} has the same linear form as in double well model

$$\psi_{phas} = \eta\phi. \tag{1.26}$$

1.3.3 Landau model

This model is adopted from the paper [3] and [4] and the Landau theory from paper [5]. The Landau theory for chemical energy of phase transformation is utilized here. The model combines the phase energy and the potential barrier energy and is referred to as chemical energy

$$\psi_{chem} = \psi_{phas} + \psi_{bar}. \tag{1.27}$$

The assumption of The Landau theory of phase transition is that the phase field variable η is small and uniform. Than the chemical part of the energy density can be approximated as a power series in η. General expansion for a single phase field variable, if we consider an internal or external field H is given by

$$\psi_{chem} = H\eta + \frac{A}{2}\eta^2 - \frac{B}{3}\eta^3 + \frac{C}{4}\eta^4 \tag{1.28}$$

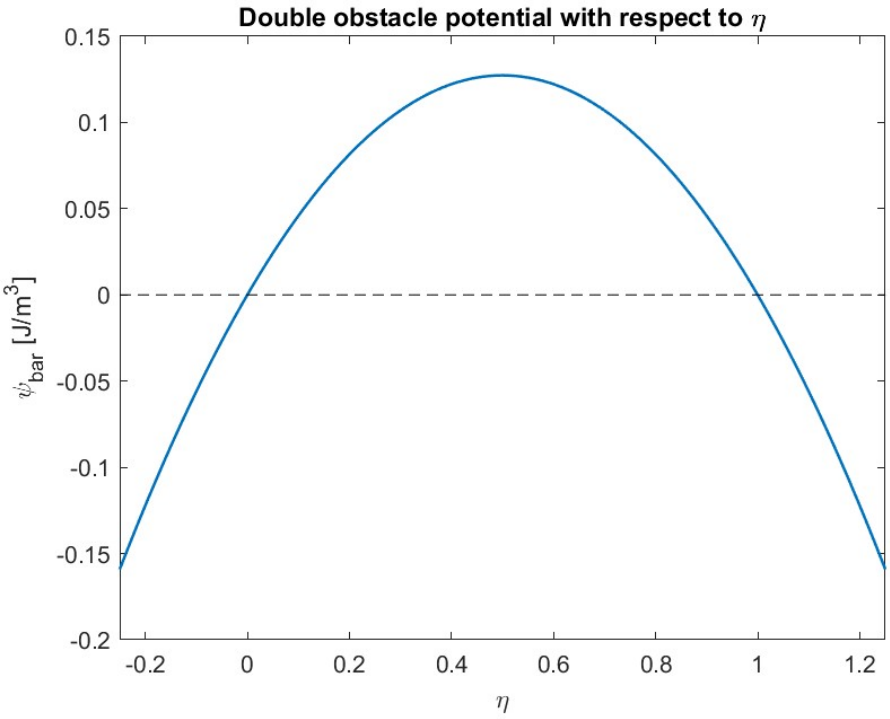

Figure 1.3: Double obstacle potential ψ_{bar} as a function of the phase field variable η. We set the constant $\ell = 0.5$ nm, $\gamma = 0.2$ J/m^2.

In following we assume that $H = 0$. Here, in our model, the constants are defined as $A = 24\gamma/\delta$, $B = 3A - 12\phi$ and $C = 2A - 12\phi$. Parameter δ determine the thickness of interface. In Subsec. 1.7.1, we demonstrate that γ represents also the interface energy per unit area. ϕ is the difference in the phase energy between β and ω phase. Indeed, if we set $\eta = 1$ we obtain

$$\phi = \frac{A}{2} - \frac{B}{3} + \frac{C}{4} \tag{1.29}$$

from definition of constants B and C. By direct computation, we obtain that ψ_{chem} has a minimum in $\eta = 0$ and $\eta = 1$, see Fig. 1.5. Due to this fact in the implementation, similar to the double well model, their values are automatically constraining between 0 and 1. However, the disadvantage is a difficult study of the phase interface because the connection of these two energies together poses difficulties in approximating its shape. But it is possible to decompose the density of chemical energy into the densities of phase and barrier energy using the definitions of the constants B and C as follows

$$\psi_{bar} = \frac{A}{2}(\eta^2 - 2\eta^3 + \eta^4) = \frac{A}{2}\eta^2(\eta - 1)^2, \tag{1.30}$$

which is the same barrier energy as in double well, except the constant $A/2$. In this model we obtain non-linear mixing of phase energy

$$\psi_{phas} = (4\eta^3 - 3\eta^4)\phi. \tag{1.31}$$

After this decomposition, it is possible to compute interface properties similarly to the double well model.

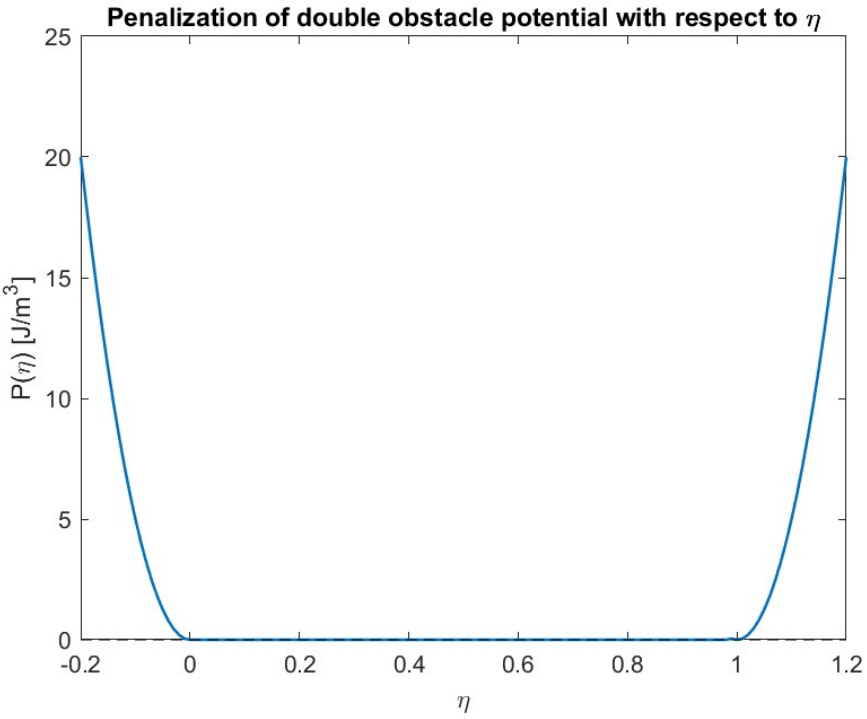

Figure 1.4: Penalization $P(\eta)$

The gradient energy we define as

$$\psi_{grad} = \frac{\beta}{2}|\nabla\eta|^2, \tag{1.32}$$

where $\beta = 3\gamma\delta/2$.

1.4 Models for more variants of ω

1.4.1 Double obstacle

In the case of more phases, according to paper [6], we introduce $N+1$ phase field variables $\eta_i, i = 0, 1, \cdots, N$. Here, the phase field variable η_0 corresponds to the parent phase β, and the remaining variables η_i correspond to different variants of the ω_i. The generalized double obstacle potential by itself also does not maintain the values of phase variables between 0 and 1. Therefore, we require that all phase field variables have to be positive and its sum, including η_0, must be equal to 1. We require the following constraint among the phase field variables η_i

$$0 \leq \eta_i, \text{ for } i = 0, 1, \ldots, N \quad \text{and} \quad \sum_{i=0}^{N} \eta_i = 1. \tag{1.33}$$

This restriction above implies that the phase field variables are bounded between 0 and 1. Which is achieved thanks to penalization and replacing the phase field variable η_0 corresponding to parent phase β with other phase field variables $\eta_i, i = 1, 2, \cdots, N$

$$P_i(\eta_i) = \begin{cases} \frac{1}{2}c\eta_i^2 & \eta_i < 0, \\ 0 & \eta_i > 0 \quad \text{for all} \quad i = 0, 1, \ldots, N, \end{cases} \tag{1.34}$$

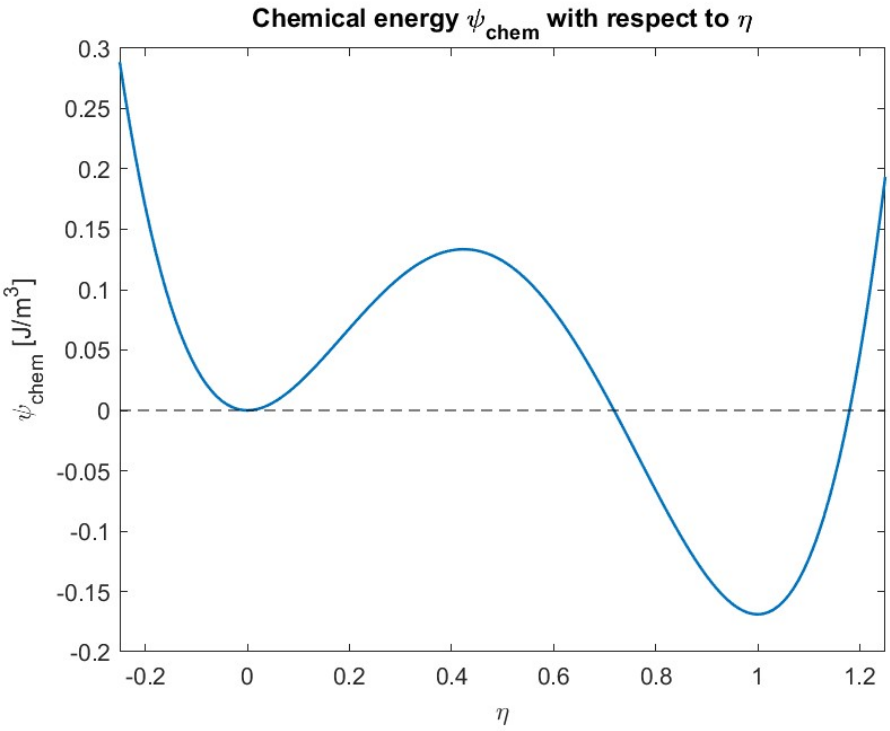

Figure 1.5: Chemical energy ψ_{chem} as a function of the phase field variable η. We set the constant $A = 5.6549$ J/m^3, $B = 18.9926$ J/m^3, $C = 13.3377$ J/m^3

where

$$\eta_0 = 1 - \sum_{i=1}^{N} \eta_i. \tag{1.35}$$

According to paper [7], we can generalize interface energy (1.24) for multiple phases as follows

$$\psi_{int} = \sum_{i=0}^{N} \sum_{j>i}^{N} \frac{4\gamma_{ij}}{\pi \ell_{ij}} \left(\eta_i \eta_j - \ell_{ij}^2 \nabla \eta_i \cdot \nabla \eta_j \right), \tag{1.36}$$

where γ_{ij} denotes the interface energy between phases i and j, and ℓ_{ij} is the thickness parameter between phases i and j such that $\pi \ell_{ij}$ is the thickness in a stress-free state. If the parameters ℓ_{ij} and γ_{ij} satisfy following equality (1.37) and (1.38), than it is possible to simplify the formulae (1.36). We need

$$\ell_{0j} = \ell_{\beta\omega} \quad \text{and} \quad \gamma_{0j} = \gamma_{\beta\omega} \text{ for } i = 0, \quad j = 1, 2, \ldots, N, \tag{1.37}$$

where the parameters $\ell_{\beta\omega}$ and $\gamma_{\beta\omega}$ denote the thickness and energy density, respectively, between the β phase and any arbitrary ω phase. Parameters between ω phases are all the same

$$\ell_{ij} = \ell_{\omega\omega} \quad \text{and} \quad \gamma_{ij} = \gamma_{\omega\omega} \quad \text{for} \quad i, j = 1, 2, \ldots, N, \tag{1.38}$$

where the parameters $\ell_{\omega\omega}$ and $\gamma_{\omega\omega}$ denote the thickness and energy density, respectively, between the ω phases.

The sum (1.36) can be divided into two parts. For $i = 0$ we obtain

$$\sum_{j=1}^{N} \frac{4\gamma_{0j}}{\pi\ell_{0j}} \left(\eta_0\eta_j - \ell_{0j}^2 \nabla\eta_0 \cdot \nabla\eta_j\right) =$$
$$\frac{4\gamma_{\beta\omega}}{\pi\ell_{\beta\omega}} \left(\eta_0 \sum_{j=1}^{N} \eta_j - \ell_{\beta\omega}^2 \nabla\eta_0 \cdot \nabla \left(\sum_{j=1}^{N} \eta_j\right)\right) = \frac{4\gamma_{\beta\omega}}{\pi\ell_{\beta\omega}} \left(\eta_0(1-\eta_0) + \ell_{\beta\omega}^2 |\nabla\eta_0|^2\right), \tag{1.39}$$

in the second equality we use the restriction (1.33) in the form

$$\sum_{j=1}^{N} \eta_j = 1 - \eta_0. \tag{1.40}$$

From the second part of the sum for $i = 1, 2, \ldots, N$ one gets

$$\sum_{i=1}^{N} \sum_{j>i}^{N} \frac{4\gamma_{ij}}{\pi\ell_{ij}} \left(\eta_i\eta_j - \ell_{ij}^2 \nabla\eta_i \cdot \nabla\eta_j\right) =$$
$$\sum_{i=1}^{N} \sum_{j=1}^{N} \frac{2\gamma_{ij}}{\pi\ell_{ij}} \left(\eta_i\eta_j - \ell_{ij}^2 \nabla\eta_i \cdot \nabla\eta_j\right) - \sum_{i=1}^{N} \frac{2\gamma_{ii}}{\pi\ell_{ii}} \left(\eta_i\eta_i - \ell_{ii}^2 \nabla\eta_i \cdot \nabla\eta_i\right), \tag{1.41}$$

using the equality (1.40), the sum above is equal to

$$\frac{2\gamma_{\omega\omega}}{\pi\ell_{\omega\omega}} \left(\sum_{i=1}^{N} \ell_{\omega\omega}^2 |\nabla\eta_i|^2 - \ell_{\omega\omega}^2 |\nabla\eta_0|^2 + \sum_{i=1}^{N} \eta_i((1-\eta_0) - \eta_i)\right) =$$
$$\frac{2\gamma_{\omega\omega}}{\pi\ell_{\omega\omega}} \left(\eta_0(1-\eta_0) - \ell_{\omega\omega}^2 |\nabla\eta_0|^2 + \sum_{i=1}^{N} \ell_{\omega\omega}^2 |\nabla\eta_i|^2 + \sum_{i=1}^{N} \eta_i(1-\eta_i)\right). \tag{1.42}$$

For concise notation, let us define the following constants

$$\omega_0 = \frac{4\gamma_{\beta\omega}}{\pi\ell_{\beta\omega}} - \frac{2\gamma_{\omega\omega}}{\pi\ell_{\omega\omega}}, \qquad \varepsilon_0 = \frac{4\gamma_{\beta\omega}\ell_{\beta\omega}}{\pi} - \frac{2\gamma_{\omega\omega}\ell_{\omega\omega}}{\pi},$$
$$\omega_i = \frac{2\gamma_{\omega\omega}}{\pi\ell_{\omega\omega}}, \qquad \varepsilon_i = \frac{2\gamma_{\omega\omega}\ell_{\omega\omega}}{\pi}.$$

Finally, by adding the results of (1.39) and (1.42), we obtain the following equality

$$\psi_{int} = \omega_0\eta_0(1-\eta_0) + \varepsilon|\nabla\eta_0|^2 + \sum_{i=1}^{N} \omega_i\eta_i(1-\eta_i) + \varepsilon_i|\nabla\eta_i|^2. \tag{1.43}$$

Which is suitable formula for numerical implementation. These parameters allow us to chose different properties of the interfaces between two ω phases, or between β and ω.

The phase energy ψ_{phas} is defined as the weighted sum of the phase energies ϕ_i of individual phases ω_i

$$\psi_{phas} = \sum_{i=1}^{N} \eta_i\phi_i. \tag{1.44}$$

Unlike the Landau model described below, this phase energy mixing is also linear.

1.4.2 Landau model

For N variants of the ω_i phases, $i = 1, 2, \cdots, N$ the chemical energy of the system is given by

$$\psi_{chem}(\eta_1, \eta_1, \cdots, \eta_N) = \frac{A}{2}\left(\sum_{i=1}^{N}\eta_i^2\right) - \frac{B}{3}\left(\sum_{i=1}^{N}\eta_i^3\right) + \frac{C}{4}\left(\sum_{i=1}^{N}\eta_i^2\right)^2. \tag{1.45}$$

Recall, that $A = 24\gamma/\delta, B = 3A - 12\phi$ and $C = 2A - 12\phi$. Parameter δ determine the thickness of interface, ϕ is the difference in the phase energy between β and arbitrary ω_i phase (all variants of ω phases have the same energy difference, in this model). Parameter γ determine the interface energy per unit area, as shown in Subsec. 1.7.1. Similarly to the case of a single phase, we can decompose the density of chemical energy into the densities of phase and barrier energy using the definitions of the constants B and C as follows

$$\psi_{phas} = 4\left(\sum_{i=1}^{N}\eta_i^3\right)\phi - 3\left(\sum_{i=1}^{N}\eta_i^2\right)^2\phi, \tag{1.46}$$

and

$$\psi_{bar} = \frac{A}{2}\left(\sum_{i=1}^{N}\eta_i^2 - 2\sum_{i=1}^{N}\eta_i^3 + \left(\sum_{i=1}^{N}\eta_i^2\right)^2\right). \tag{1.47}$$

It is easy to verify that the equality $\psi_{chem} = \psi_{phas} + \psi_{bar}$ holds. Again, non-linear mixing occurs in the phase energy density, which is not present in either the double well or double obstacle models. In this model, unlike the double obstacle model, it is not possible to select the energies or thickness of individual phase interfaces, and the same applies to the phase energy between β and i-th variants of ω. It would be good to develop a model that allows for this.

Gradient energy can be written as

$$\psi_{grad} = \frac{1}{2}\sum_{p=1}^{N}\sum_{i=1}^{3}\sum_{j=1}^{3}\beta_{ij}\frac{\partial\eta_p}{\partial x_i}\frac{\partial\eta_p}{\partial x_j}, \tag{1.48}$$

where β_{ij} is identity tensor multiplied by constant β due to the isotropic interface properties. Thus it can be written as

$$\psi_{grad} = \frac{\beta}{2}\sum_{p=1}^{N}|\nabla\eta_p|^2, \tag{1.49}$$

where β is

$$\beta = \frac{3\gamma\delta}{2}. \tag{1.50}$$

The model is defined by specifying constants γ, δ and ϕ (and elastic parameters). It can be used to compare this model with the double obstacle model in numerical implementation. We can set the same phase energy difference $\phi = \phi_i$ for all i and interface energy γ. The relation between δ and ℓ is determined later based on the velocity of propagation of the ω phase.

1.5 Elastic energy

For all three described models, we use the same elastic energy ψ_{el}. For one variant of ω phase we use only first bain strain tensor $\mathbf{U}_1^t$.

Elastic energy arises from stress induced by deformation from bain strain $\mathbf{U}^t$ to total strain ϵ. The bain strain $\mathbf{U}^t$ is induced by the deformation of the crystalline lattice when the ω phase appears. The bain strain $\mathbf{U}^t$ is given by linear combination of bain strain tensors $\mathbf{U}_i^t$, $i = 1, 2, \cdots, N$ corresponding to the i-th variant of the ω_i phase

$$\mathbf{U}^t(\eta_i) = \sum_{i=1}^{N} \eta_i \mathbf{U}_i^t. \tag{1.51}$$

The elastic strain ϵ^{el} can be written as

$$\epsilon^{el}(\eta_i, \nabla \boldsymbol{u}) = \epsilon(\nabla \boldsymbol{u}) - \mathbf{U}^t(\eta_i). \tag{1.52}$$

Then the stress tensor σ has the form

$$\sigma = \frac{E}{1+\nu}\left[\epsilon^{el} + \frac{\nu}{1-2\nu}\mathrm{tr}(\epsilon)\mathbb{I}\right], \tag{1.53}$$

Then the elastic energy for this model is defined as

$$\psi_{el} = \frac{E}{2(1+\nu)}\left[|\epsilon^{el}|^2 + \frac{\nu}{1-2\nu}\mathrm{tr}^2(\epsilon^{el})\right]. \tag{1.54}$$

Hence, we can write our equilibrium condition as

$$\nabla \cdot \frac{\partial \psi_{el}}{\partial \nabla \boldsymbol{u}} = 0, \tag{1.55}$$

which is $\nabla \cdot \sigma = 0$.

1.6 Governing equations

The evolution of the phase field variables $\eta_i, i = 1, 2, \cdots, N$, where N is the number of phases ω_i, can be modeled using the time-dependent Ginzburg-Landau equation, as postulated in the paper [8]. For the displacement $\boldsymbol{u}$, we have the equilibrium condition (1.55). Altogether, we have the following equations

$$\frac{\partial \eta_i}{\partial t} = -L\frac{\delta \Psi}{\delta \eta_i(\boldsymbol{r}, t)}, \tag{1.56}$$

$$\nabla \cdot \sigma = 0, \tag{1.57}$$

$$\sigma \cdot \boldsymbol{n} = 0 \quad \text{and} \quad \frac{\partial \eta_i}{\partial \boldsymbol{n}} = 0 \quad \text{on} \quad \partial\Omega, \tag{1.58}$$

where Ψ represents the total body energy (1.1), $\boldsymbol{n}$ is normal vector to the boundary of Ω, $\eta_i(\boldsymbol{r}, t)$ denote a phase field variables, which depends on the spatial vector $\boldsymbol{r} = (x, y, z)$ and L is a mobility parameter. The symbol $\delta\Psi/\delta\eta_i$ represents the functional derivative

$$\frac{\delta \Psi}{\delta \eta_i(\boldsymbol{r}, t)} = \frac{\partial \psi}{\partial \eta_i} - \nabla \cdot \frac{\partial \psi}{\partial \nabla \eta_i}. \tag{1.59}$$

Here $\psi := \psi(\boldsymbol{\eta}, \nabla\boldsymbol{\eta}, \nabla\boldsymbol{u})$ and $\boldsymbol{\eta} = (\eta_1, \eta_2, \cdots, \eta_N)$ describes energy density ψ. The functions $\eta_i(\boldsymbol{r}, t)$ and $\boldsymbol{u}(\boldsymbol{r}, t)$ depend on time and the spatial vector.

1.6.1 Equivalent problem

We want to formulate equations (1.56) and (1.57) in terms of minimizing an appropriate functional Π

$$\Pi = \dot{\Psi} + \mathcal{D}. \tag{1.60}$$

Where $\mathcal{D}$ is called dissipation and has the form

$$\mathcal{D} = \int_\Omega \frac{1}{2L} \sum_{i=1}^{N} \dot{\eta_i}^2 \, dV. \tag{1.61}$$

Let us show that equations

$$\frac{\delta \Pi}{\delta \dot{\eta}_i} = 0, \quad \frac{\delta \Pi}{\delta \dot{\boldsymbol{u}}} = \boldsymbol{0}, \tag{1.62}$$

are equivalent to equations (1.56) and (1.57). Firstly, we can calculate the first time derivative energy density $\psi(\boldsymbol{\eta}, \nabla \boldsymbol{\eta}, \nabla \boldsymbol{u})$

$$\dot{\psi} = \frac{\partial \psi}{\partial \boldsymbol{\eta}} \cdot \dot{\boldsymbol{\eta}} + \frac{\partial \psi}{\partial \nabla \boldsymbol{\eta}} : \nabla \dot{\boldsymbol{\eta}} + \frac{\partial \psi}{\partial \nabla \boldsymbol{u}} : \nabla \dot{\boldsymbol{u}}. \tag{1.63}$$

Hence $\delta \Psi / \delta \eta_i = \delta \dot{\Psi} / \delta \dot{\eta}_i$

$$\frac{\delta \dot{\Psi}}{\delta \dot{\eta}_i} = \frac{\partial \dot{\psi}}{\partial \dot{\eta}_i} + \nabla \cdot \frac{\partial \dot{\psi}}{\partial \nabla \dot{\eta}_i} = \frac{\partial \psi}{\partial \eta_i} + \nabla \cdot \frac{\partial \psi}{\partial \nabla \eta_i} = \frac{\delta \Psi}{\delta \eta_i}. \tag{1.64}$$

For functional derivative of dissipation $\mathcal{D}$ with respect to $\dot{\eta}_i$ holds

$$\frac{\delta \mathcal{D}}{\delta \dot{\eta}_i} = \frac{1}{L} \dot{\eta}_i. \tag{1.65}$$

From the result (1.64) and (1.65) we obtain equivalent formulation for equation (1.56) as

$$0 = \frac{\delta \Pi}{\delta \dot{\eta}_i} = \frac{\delta \dot{\Psi}}{\delta \dot{\eta}_i} + \frac{\delta \mathcal{D}}{\delta \dot{\eta}_i} = \frac{\delta \Psi}{\delta \eta_i} + \frac{1}{L} \dot{\eta}_i. \tag{1.66}$$

In similar way can be expressed the second equation-mechanical equilibrium condition

$$\frac{\delta \Psi}{\delta \boldsymbol{u}} = \boldsymbol{0}. \tag{1.67}$$

Note, that only elastic energy ψ_{el} depends on $\boldsymbol{u}$ or $\nabla \boldsymbol{u}$. Then one gets

$$\frac{\delta \Psi}{\delta \boldsymbol{u}} = \underbrace{\frac{\partial \psi}{\partial \boldsymbol{u}}}_{=0} + \nabla \cdot \frac{\partial \psi}{\partial \nabla \boldsymbol{u}} = \nabla \cdot \frac{\partial \psi_{el}}{\partial \nabla \boldsymbol{u}}, \tag{1.68}$$

and from formula for elastic energy (1.54) it is easy to calculate

$$\frac{\partial \psi_{el}}{\partial \nabla \boldsymbol{u}} = \sigma. \tag{1.69}$$

Hence we obtain the second equation (1.57) in the form of functional derivative Ψ with respect to $\boldsymbol{u}$

$$\frac{\delta \Psi}{\delta \boldsymbol{u}} = \nabla \cdot \frac{\partial \psi_{el}}{\partial \nabla \boldsymbol{u}} = \nabla \cdot \sigma = 0. \tag{1.70}$$

Moreover, we have

$$\frac{\delta\Psi}{\delta\boldsymbol{u}} = \frac{\delta\dot{\Psi}}{\delta\dot{\boldsymbol{u}}} = \frac{\delta\dot{\Psi}}{\delta\dot{\boldsymbol{u}}} + \frac{\delta\mathcal{D}}{\delta\dot{\boldsymbol{u}}} = \frac{\delta\Pi}{\delta\dot{\boldsymbol{u}}}. \tag{1.71}$$

The first equality follows from time derivative of ψ, see (1.63), the second equality holds because dissipation $\mathcal{D}$ does not depend on displacement (1.61) and last equality is from definition of functional Π, see (1.60).

Now we can formulate the equations (1.56) and (1.57) in terms of finding minimum of functional Π:

$$\forall t > t_0 \text{ find } \min_{\dot{\boldsymbol{u}},\dot{\boldsymbol{\eta}}} \Pi[\dot{\boldsymbol{u}}, \dot{\boldsymbol{\eta}}], \tag{1.72}$$

where $\Pi[\dot{\boldsymbol{u}}, \dot{\boldsymbol{\eta}}] = D[\dot{\boldsymbol{\eta}}] + \dot{\Psi}[\dot{\boldsymbol{u}}, \dot{\boldsymbol{\eta}}]$ are functionals. In fact, we are not looking for the minimum of Π, but we are seeking stationary points that correspond to the solutions of the Euler-Lagrange equations.

1.7 Analytic benchmark

In this section, we compute several semi-analytical results that we verify in the next chapter. We are able to derive the shape and energy of the interface, the minimum grain size required for its growth, and the rate of interface propagation in two specific cases.

1.7.1 Interface properties

Suitable choice of interface energy ψ_{int} in double obstacle and double well allows to compute a function approximating the shape of the sharp interface between two phases. In Landau model we firstly have to separate ψ_{bar} from chemical energy. Let us note before the computation that the elastic and phase energy can be neglected, as they are orders of magnitude smaller than ψ_{int} at the interface of the two phases. Moreover, the approximating function have to minimize the one dimensional functional

$$\min_{\eta:\eta\in[0,1]} \int_{-\infty}^{\infty} \psi_{int}(\eta(x), \eta'(x))\, dx, \tag{1.73}$$

where

$$\psi_{int}(\eta(x), \eta'(x)) = \psi_{bar}(\eta(x)) + \psi_{grad}(\eta'(x)). \tag{1.74}$$

We require the function $\eta(x)$ to satisfy

$$\lim_{x\to-\infty} \eta(x) = 0, \quad \eta(0) = \frac{1}{2}, \quad \text{and} \quad \lim_{x\to\infty} \eta(x) = 1. \tag{1.75}$$

For a general model, if gradient energy can be expressed in the form $\psi_{grad} = \kappa|\nabla\eta|^2$, where κ is suitable constant, it leads to the Euler-Lagrange equation, with the form

$$\frac{\partial\psi_{bar}}{\partial\eta} = 2\kappa\left(\frac{\partial^2\eta(x)}{\partial x^2}\right). \tag{1.76}$$

It is possible to find the first integral of this equation, which can simplify further calculations

$$\psi_{bar}(\eta(x)) = \kappa\left(\frac{\partial\eta(x)}{\partial x}\right)^2. \tag{1.77}$$

In one dimension, we find that the gradient and barrier energies satisfying (1.73) are equal

$$\psi_{bar} = \psi_{grad}. \tag{1.78}$$

From this formula it is possible to solve the Euler-Lagrange equation by separation of variables to give the profile of planar interface, with the condition (1.75)

$$\int 1\, dx = \int \sqrt{\frac{\kappa}{\psi_{bar}(\eta)}}\, d\eta. \tag{1.79}$$

Or we can simply compute the interface energy γ as

$$\gamma = \int_{-\infty}^{\infty} \psi_{int}(\eta(x), \eta'(x))\, dx = \int_{-\infty}^{\infty} 2\kappa \left(\frac{\partial \eta(x)}{\partial x}\right)^2 dx = \int_0^1 2\sqrt{\kappa \psi_{bar}(\eta)}\, d\eta. \tag{1.80}$$

In the second equality we use equation (1.77) i.e. $\psi_{bar} = \psi_{grad}$, and in third equality we use $\psi_{int} = 2\psi_{bar}(\eta(x))$ and change of integration variables $\eta = \eta(x)$.

Interface properties – double obstacle

We use ψ_{int} from double obstacle (1.24). The corresponding Euler-Lagrange equation yields

$$\ell^2 \eta''(x) + \eta(x) = \frac{1}{2}. \tag{1.81}$$

The solution is

$$\eta(x) = \begin{cases} 0 & x < -\frac{\pi\ell}{2}, \\ \frac{1}{2}\left(1 + \sin\left(\frac{x}{\ell}\right)\right) & x \in \left[-\frac{\pi\ell}{2}, \frac{\pi\ell}{2}\right], \\ 1 & x > \frac{\pi\ell}{2}. \end{cases} \tag{1.82}$$

The thickness of the interface is $\pi\ell$. By substituting the function $\eta(x)$ back into the integral, we obtain the interface energy

$$\int_{-\frac{\pi\ell}{2}}^{\frac{\pi\ell}{2}} \psi_{int}(\eta(x), \eta'(x))\, dx = \int_{-\frac{\pi\ell}{2}}^{\frac{\pi\ell}{2}} \frac{\gamma}{\pi\ell}\left(\cos^2\left(\frac{x}{\ell}\right) + \left(1 - \sin^2\left(\frac{x}{\ell}\right)\right)\right) dx = \gamma. \tag{1.83}$$

Interface properties – double well

The same can be done with double well interface energy. We get the Euler-Lagrange equation

$$\frac{\ell^2}{4}\eta''(x) = 2\eta^3 - 3\eta^2 + \eta. \tag{1.84}$$

Its solution is

$$\eta(x) = \frac{1}{2}(1 + \tanh(x/\ell)). \tag{1.85}$$

interface energy is given by

$$\int_{-\infty}^{\infty} \psi_{int}(\eta(x), \eta'(x))\, dx = \gamma. \tag{1.86}$$

And ℓ determines the sharpness of interface. The result correspond with the thesis [9].

Interface properties – Landau

The chemical energy is given by (1.29)

$$\psi_{chem} = \frac{A}{2}\eta^2 - \frac{3A - 12\phi}{3}\eta^3 + \frac{2A - 12\phi}{4}\eta^4, \tag{1.87}$$

see the definition of constant B, C. If we set $\phi = 0$ we obtain ψ_{bar} separately

$$\psi_{bar} = \frac{A}{2}\eta^2 - A\eta^3 + \frac{A}{2}\eta^4 = \frac{A}{2}\eta^2(1-\eta)^2. \tag{1.88}$$

It leads to Euler-Lagrange equation in the form

$$\frac{\beta}{A}\eta''(x) = \eta(1-\eta)(1-2\eta), \tag{1.89}$$

where $\beta/A = \delta^2/16$. This equation is the same as in the case of the double well model except for the constant. The function approximating the the shape of interface is given by

$$\eta(x) = \frac{1}{2}(1 + \tanh(2x/\delta)). \tag{1.90}$$

interface energy can be computed from (1.80). After modifying the constants in the paper [4] (See definition of β), it results in the interface energy being equal to γ. Due to non-linear mixing in phase energy, unlike the previous two models, the phase energy is shifted to the right. It is possible to compute value of $\psi_{phas}(x)$ on the interface by substituting equation (1.90) into $\psi_{phas}(\eta(x))$, see Fig. 1.6. Phase energy is shifted due to non-linearity towards the ω phase. The value of this shift is $x^* = 0.102$ nm. This value is used to correct the following analytical benchmark.

1.7.2 The minimum size of the ω phase

In this section our goal is to determine critical radius r for the growth of the ω phase. We perform calculations for a single ω phase in two dimensions. Here, for the further computation, we neglect the elastic energy ψ_{el}. Assume that $\eta(\boldsymbol{r})$ is given by

$$\eta(\boldsymbol{r}) = \begin{cases} 1 & |\boldsymbol{r}| < r, \\ 0 & |\boldsymbol{r}| \geq r. \end{cases} \tag{1.91}$$

We do certain approximations. Firstly, we neglect the specific shape of the interface. Then, the total phase energy can be expressed as $\pi r^2\phi$ (The area of phase occurrence times ϕ). The second approximation involves assuming that the circular interface possesses the same energy density γ per unit area as the planar interface. Consequently, the total interface energy is given by $2\pi r\gamma$ (The length of the interface times γ). Therefore, the total energy Ψ can be computed as

$$\Psi = \int_\Omega \left(\psi_{int} + \psi_{phas}\right) dV = 2\pi r\gamma + \pi r^2\phi. \tag{1.92}$$

As the total energy Ψ is determined only by single parameter r the functional derivative reduce only on partial derivative with respect to r. One can observe

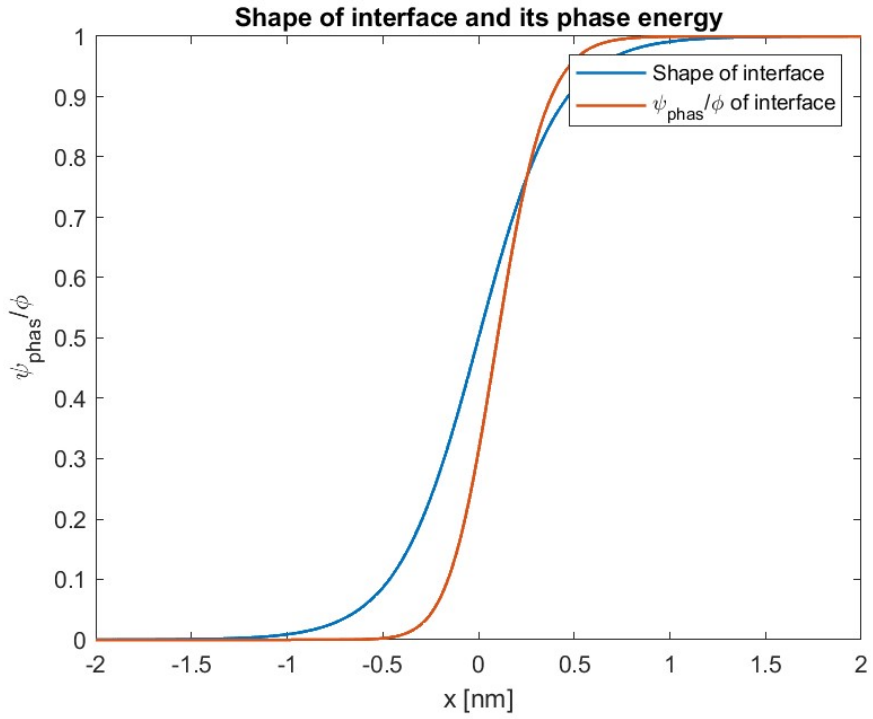

Figure 1.6: Normalized phase energy $\frac{\psi_{phas}}{\phi}$ in comparison with the interface shape. We use $\delta = 0.849$ nm.

the dependence of the total energy Ψ of the system on the size of the ω phase in Fig. 1.7. We can find the maximum of the energy

$$0 = \frac{\partial \Psi}{\partial r} = 2\pi\gamma + 2\pi\phi r. \tag{1.93}$$

Hence, the maximum energy occurs for

$$r = -\frac{\gamma}{\phi}. \tag{1.94}$$

If $r < \gamma/\phi$, then r will decrease because according to equation (1.56), the system evolves in the direction of the greatest energy minimization. On the other hand if $r > \gamma/\phi$, than r will increase.

To determine the critical radius of the ω phase in three dimensions, we can use the same approach. Hence, in three dimensional space, the total energy Ψ is given by

$$\Psi = \int_{\Omega} (\psi_{int} + \psi_{phas})\, dV = 4\pi r^2\gamma + \frac{4}{3}\pi r^2\phi. \tag{1.95}$$

And the critical radius is

$$r = -\frac{2\gamma}{\phi}. \tag{1.96}$$

Note that due to the shift of phase energy in the Landau model, the corrected value of critical radius in two dimensions is

$$r_L = -\frac{\gamma}{\phi} + x^*, \tag{1.97}$$

because $\psi_{phas} = \pi(r - x^*)^2\phi$.

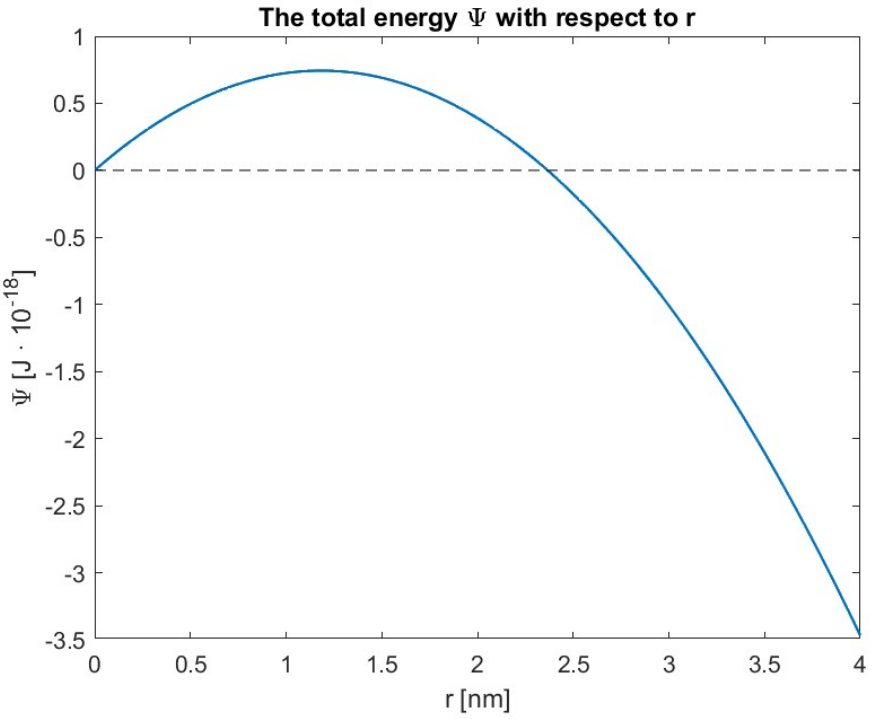

Figure 1.7: Energy of the system with respect to size of the ω phase. We use $\phi = -0.169$ J/m^3 and $\gamma = 0.2$ J/m^2.

1.7.3 The rate of interface propagation

We want to approximate speed of β to ω transformation. Consider the model setting in two dimension where we have only interface energy ψ_{int}, phase energy ψ_{phas} and dissipation. The distribution of the ω and β phase see on Figure below. The interface is oriented at 45 degrees, and its position along the ξ axis that is perpendicular to the interface is specified by $\xi = \zeta$ with $\xi = 0$ corresponding to the vertex. The length of the interface is thus 2ζ (dashes line on the picture). Therefore, the total interface energy Ψ_{int} is equal to

$$\Psi_{int} = 2\zeta\gamma. \tag{1.98}$$

And the total phase energy is equal to

$$\Psi_{phas} = -\zeta^2\phi, \tag{1.99}$$

where ζ^2 is the area of the triangle with β phase.

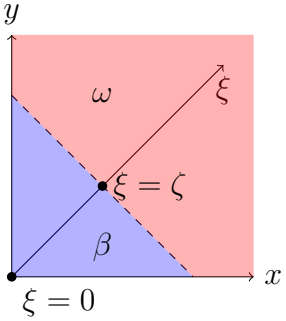

Distribution of β and ω phase in square

The movement of the interface towards the origin $\xi = 0$ decreases the total energy $\Psi_{int} + \Psi_{phas}$ because $\phi < 0$, thus indicating the presence of a nonzero driving force for this evolution. We define the propagation speed v_n as a vector perpendicular to the interface such that $|v_n| = \dot{\zeta} \sim \dot{\eta}$. This allows us to calculate the density of dissipation per unit area $\dot{\eta}/(2L)$. The profile of the diffuse interface with its center located at $\xi = \zeta(t)$ is given by $\eta(\xi - \zeta(t))$ where $\eta(\xi)$ is calculated in Subsec. 1.7.1. And its time derivative for double obstacle $\dot{\eta}_D$ and Landau $\dot{\eta}_L$ model is given by

$$\dot{\eta}_D = -\frac{\dot{\zeta}}{2l}\cos\left(\frac{\xi-\zeta}{l}\right),$$
$$\dot{\eta}_L = -\frac{\dot{\zeta}}{\delta}\mathrm{sech}^2\left(\frac{2(\xi-\zeta)}{\delta}\right).$$

And dissipation per unit area is

$$\mathcal{D}_D = \int_{\zeta-\frac{\pi\ell}{2}}^{\zeta+\frac{\pi\ell}{2}} \frac{\dot{\eta}_D^2}{2L} d\xi = \frac{\pi\dot{\zeta}^2}{16L\ell},$$
$$\mathcal{D}_L = \int_{-\infty}^{\infty} \frac{\dot{\eta}_L^2}{2L} d\xi = \frac{\dot{\zeta}^2}{3L\delta}.$$

Hence, our functional Π is given by (1.60)

$$\Pi_D = \dot{\Psi}_{int} + \dot{\Psi}_{phas} + 2\zeta\mathcal{D}_D = 2\dot{\zeta}\gamma - 2\zeta\dot{\zeta}\phi + \frac{\pi\dot{\zeta}^2\zeta}{8L\ell},$$
$$\Pi_L = \dot{\Psi}_{int} + \dot{\Psi}_{phas} + 2\zeta\mathcal{D}_L = 2\dot{\zeta}\gamma - 2\zeta\dot{\zeta}\phi + \frac{2\dot{\zeta}^2\zeta}{3L\delta}.$$

$\dot{\zeta}$ can be computed in both situations from the following equations

$$\frac{\delta\Pi_D}{\delta\dot{\zeta}} = 0 \quad \text{and} \quad \frac{\delta\Pi_L}{\delta\dot{\zeta}} = 0, \tag{1.100}$$

and the propagation speeds are given by

$$\dot{\zeta}_D = \frac{8L\ell}{\pi\zeta}(\zeta\phi - \gamma) \quad \text{and} \quad \dot{\zeta}_L = \frac{3L\delta}{2\zeta}(\zeta\phi - \gamma). \tag{1.101}$$

This approach can be generalized to the distribution of ω in a circle. Assume the distribution in circle with the radius equal to r, see Figure below.

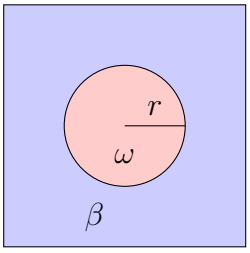

Distribution of β and ω phase in circle

And define $\dot{\eta} \sim \dot{r} = |v_n|$, where v_n is the propagation speed defined above. Let us assume the same dissipation potentials per unit area $\mathcal{D}_D$ and $\mathcal{D}_L$ as for the planar interface. The total dissipation is obtained by multiplying each by $2\pi r$. The total energy is the same for both models, given by

$$\Psi_{int} + \Psi_{phas} = 2\pi r\gamma + \pi r^2\phi. \tag{1.102}$$

From equations (1.100) we obtain the results

$$\dot{r}_D = -\frac{8L\ell}{\pi r}(r\phi + \gamma) \quad \text{and} \quad \dot{r}_L = -\frac{3L\delta}{2r}(r\phi + \gamma). \tag{1.103}$$

For $\dot{r} = 0$ we obtain the critical radius. In both cases, the contribution from the phase energy aids the growth of the ω phase because $\phi < 0$. Conversely, the contribution from the interface energy in the first corner situation accelerates the phase propagation because the expansion of the phase leads to a decrease in the length of the interface. In the second situation on the circle, it slows down the growth of the phase because with its growth, the length of the interface increases. The evolution of radius r and distance ζ can be computed by separation of constant, but expressing the variables with respect to the time is difficult.

When we set

$$\delta = \frac{16\ell}{3\pi}, \tag{1.104}$$

the propagation speed of planar interface is equal for both models. Note that due to the shift of phase energy in the Landau model, the corrected equation for $\dot{r}_L$ is

$$\dot{r}_L = -\frac{3L\delta}{2r}((r - x^*)\phi + \gamma), \tag{1.105}$$

because $\psi_{phas} = \pi(r - x^*)^2\phi$.

2. Numerical solution of chosen problem

2.1 Numerical scheme

2.1.1 Discretization in time

Recall that we are solving the equation (1.72)

$$\forall t > t_0 \text{ find } \min_{\dot{\boldsymbol{u}},\dot{\boldsymbol{\eta}}} \int_\Omega \left(\frac{1}{2L} \sum_{i=1}^{N} \dot{\eta_i}^2 + \dot{\psi}(\boldsymbol{\eta}, \nabla\boldsymbol{\eta}, \nabla\boldsymbol{u}) \right) dV. \tag{2.1}$$

The time derivative of $\dot{\boldsymbol{\eta}}$ is discretized using the Euler scheme, i.e.

$$\dot{\boldsymbol{\eta}} = \frac{\boldsymbol{\eta}_t - \boldsymbol{\eta}_{t-\tau}}{\tau}, \tag{2.2}$$

where τ is time step. Here and in the following, we use subscript notation $\boldsymbol{\eta}_t$ to denote the value of the function $\boldsymbol{\eta}$ at time t. Therefore, the density of dissipation takes this form

$$\frac{1}{2L} \sum_{i=1}^{N} \dot{\eta_i}^2 \approx \frac{1}{2L\tau^2} |\boldsymbol{\eta}_t - \boldsymbol{\eta}_{t-\tau}|^2. \tag{2.3}$$

Using this Euler scheme, one gets the approximation $\tilde{\mathcal{D}}$ of the dissipation $\mathcal{D}$

$$\tilde{\mathcal{D}} = \int_\Omega \frac{1}{2L\tau^2} |\boldsymbol{\eta}_t - \boldsymbol{\eta}_{t-\tau}|^2 \, dV. \tag{2.4}$$

In a similar way, we discretize the time derivative of $\dot{\psi}(\boldsymbol{\eta}, \nabla\boldsymbol{\eta}, \nabla\boldsymbol{u})$

$$\dot{\psi} = \frac{\psi_t - \psi_{t-\tau}}{\tau}. \tag{2.5}$$

And from linearity of integral one gets approximation of time derivative of total energy $\dot{\Psi}$

$$\dot{\Psi} \approx \frac{\Psi_t - \Psi_{t-\tau}}{\tau}. \tag{2.6}$$

Hence, we approximate the functional Π by

$$\Pi \approx \frac{\Psi_t - \Psi_{t-\tau}}{\tau} + \tilde{\mathcal{D}}. \tag{2.7}$$

Let us note that we are seeking the minimizer of the functional Π for all t, then the functional derivative of Π is equal to zero, so we can multiply the functional by the value of time step τ, we obtain

$$\tau\Pi \approx \Psi_t - \Psi_{t-\tau} + \int_\Omega \frac{1}{2L\tau} |\boldsymbol{\eta}_t - \boldsymbol{\eta}_{t-\tau}|^2 \, dV. \tag{2.8}$$

The energy density in the previous step $\psi_{t-\tau}$ is a known function, which depends only on spatial vector $\boldsymbol{r}$. Therefore, functional derivative of $\Psi_{t-\tau}$ is equal to zero,

and we can define a new functional that we minimize, yielding the same results. It has the form

$$\tilde{\Pi} = \Psi_t + \tau\tilde{\mathcal{D}}. \tag{2.9}$$

Then for each time step we solve the following problem

$$\text{find } \min_{\boldsymbol{u}_t,\boldsymbol{\eta}_t} \int_\Omega \left(\psi(\boldsymbol{\eta}_t, \nabla\boldsymbol{\eta}_t, \nabla\boldsymbol{u}_t) + \frac{1}{2L\tau}|\boldsymbol{\eta}_t - \boldsymbol{\eta}_{t-\tau}|^2\right) dV, \tag{2.10}$$

where $\boldsymbol{\eta}_{t-\tau}$ is known function from previous time step.

2.1.2 Weak formulation

The problem (2.10) we can rewrite as

$$\frac{\delta(\Psi + \tilde{\mathcal{D}})}{\delta\eta_i} = 0 \quad \text{for } i = 1, 2 \dots N, \tag{2.11}$$

$$\frac{\delta\Psi_{el}}{\delta\boldsymbol{u}} = 0, \tag{2.12}$$

because only elastic part of the energy depends on $\boldsymbol{u}$. One can obtain the weak form of (2.11) with test functions $\varphi_i \in C^1(\Omega)$, for $i = 1, 2, \dots, N$ and almost all $t \in (0, T]$ as

$$\begin{aligned}
0 &= \int_\Omega \frac{\delta\Psi + \tilde{\mathcal{D}}}{\delta\eta_i}\varphi_i \, dV \\
&= \int_\Omega \left(\frac{1}{L}\frac{\partial\eta_i}{\partial t} + \frac{\partial\psi}{\partial\eta_i} - \nabla\cdot\frac{\partial\psi}{\partial\nabla\eta_i}\right)\varphi_i \, dV \\
&= \int_\Omega \left(\frac{1}{L}\frac{\partial\eta_i}{\partial t} + \frac{\partial\psi}{\partial\eta_i} - 2\kappa\Delta\eta_i\right)\varphi_i \, dV \\
&= \int_\Omega \left(\left(\frac{1}{L}\frac{\partial\eta_i}{\partial t} + \frac{\partial\psi}{\partial\eta_i}\right)\varphi_i + 2\kappa\nabla\eta_i\cdot\nabla\varphi_i\right) dV - \underbrace{2\kappa\int_{\partial\Omega}(\varphi_i\nabla\eta_i)\cdot \, dS}_{=0}.
\end{aligned}$$

In the third equality, we utilize that only the density of the gradient energy depends on $\nabla\eta_i$, and we use its general form $\psi_{grad} = \kappa|\nabla\eta_i|^2$ as provided in Subsec. 1.7.1. In the final equality, we employ integration by parts. The planar integral over boundary of Ω is zero due to boundary condition (1.58). Equation (2.12) is tested with $\boldsymbol{\varrho} \in C^1(\Omega, \mathbb{R})^3$ and the weak form is obtained as

$$\begin{aligned}
0 &= \int_\Omega \frac{\delta\Psi_{el}}{\delta\boldsymbol{u}}\cdot\boldsymbol{\varrho} \, dV \\
&= \int_\Omega (\nabla\cdot\sigma)\cdot\boldsymbol{\varrho} \, dV \\
&= \underbrace{\int_{\partial\Omega}(\boldsymbol{\varrho}\cdot\sigma\cdot\boldsymbol{n}) \, dS}_{=0} - \int_\Omega \sigma\colon\nabla\boldsymbol{\varrho} \, dV.
\end{aligned}$$

In the second equality we use relation (1.70). In third equality we employ integration by parts. Owing to the boundary condition, the planar integral over the boundary of Ω vanishes.

After temporal discretization, we are solving the following problem

$$\int_\Omega \left(\left(\frac{1}{L} \frac{\boldsymbol{\eta}_t - \boldsymbol{\eta}_{t-\tau}}{\tau} + \frac{\partial \psi}{\partial \boldsymbol{\eta}_t} \right) \cdot \boldsymbol{\varphi} + 2\kappa \nabla \boldsymbol{\eta}_t : \nabla \boldsymbol{\varphi} \right) dV = 0 \quad \forall \boldsymbol{\varphi} \in C^1(\Omega, \mathbb{R})^N,$$
$$\int_\Omega \sigma : \nabla \boldsymbol{\varrho} \, dV = 0 \quad \forall \boldsymbol{\varrho} \in C^1(\Omega, \mathbb{R})^3, \tag{2.13}$$

where $\boldsymbol{\varphi} = (\varphi_1, \varphi_2, \ldots, \varphi_N)$ denotes the vector of test functions.

2.1.3 Finite element method

We solve the problem (2.13) using Firedrake, a finite element code based on the weak form. Our domain Ω is a line segment, square or cube. The domain is divided into cells, and the unknown functions are approximated over the cells using polynomials. In our numerical implementation we use quadrilateral (square) cell shapes as depicted in the Figure.

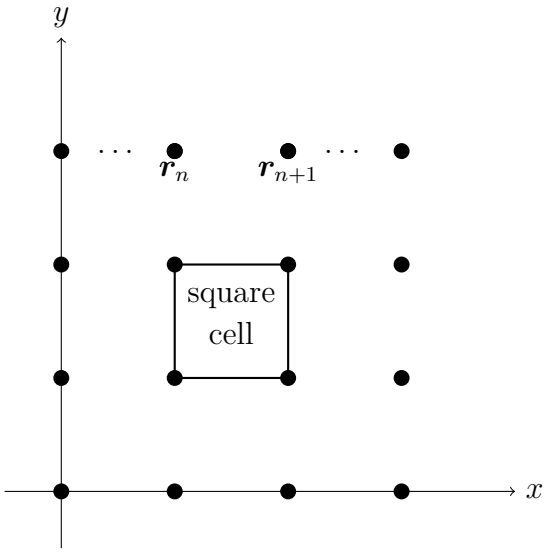

Discretization

The unknown functions over square cells are approximated using bilinear Q_1 elements. This implies that the function within each cell (in two dimensions) is approximated by a bilinear function

$$a_0 + a_1 x + a_2 y + a_3 xy. \tag{2.14}$$

The approximation of unknown functions is given by $\boldsymbol{u}_t^n = \boldsymbol{u}(\boldsymbol{r}_n, t)$ and $\boldsymbol{\eta}_t^n = \boldsymbol{\eta}(\boldsymbol{r}_n, t)$.

It is not necessary to directly compute the weak formulation, it can be computed by the *derivative* command directly by specifying the functional $\tilde{\Pi}$. The non-linear problem is solved using the Newton's method using SNES solver from PETSc library. For solving the resulting linear system, we use the direct solver MUMPS.

2.2 Benchmark results verification

This section aims to numerically verify the theoretical results of interface properties, Subsec. 1.7.1, size of the critical radius, Subsec. 1.7.2 and the phase

propagation velocity, as discussed in Subsec. 1.7.3.

2.2.1 Material parameters

The main aim of this work is to compare the Landau model with the double obstacle model, therefore we try to set the parameters similarly or equivalently based on previous theoretical calculations. The parameters γ or $\gamma_{\beta\omega}$ and ϕ or ϕ_i appear in both models and have the same meaning, so they are equal. The parameters $\ell_{\beta\omega}$ and δ are set according to equation (1.104), so that the interface propagation speeds are the same. For other parameters see Table 2.2.1. Note that the only material parameter that scales with time is the mobility parameter. Thus, in the following, we use arbitrary time without any physical units.

Constant	Value	Description
L	$1\,(\mathrm{Pa\ s})^{-1}$	Mobility parameter
γ	$0.2\,\mathrm{J/m^2}$	Equilibrium interface energy density per unit area
$\gamma_{\beta\omega}$	$0.2\,\mathrm{J/m^2}$	Equilibrium interface energy density per unit area
$\gamma_{\omega\omega}$	$0.4\,\mathrm{J/m^2}$	Equilibrium interface energy density per unit area
ℓ	$0.5\,\mathrm{nm}$	Length scale across the interface
$\ell_{\beta\omega}$	$0.5\,\mathrm{nm}$	Length scale across the interface
$\ell_{\omega\omega}$	$0.5\,\mathrm{nm}$	Length scale across the interface
δ	$0.849\,\mathrm{nm}$	Length scale across the interface
ϕ_i	$-0.169\,\mathrm{J/m^3}$	Phase energy of all ω phases in all models
β	$0.255\,\mathrm{J/m}$	Gradient coefficient
ϵ_1	-0.00162	Elasticity parameters
ϵ_2	0.00543	Elasticity parameters

Table 2.1: Overview of the material parameters and their values for double obstacle model.

2.2.2 Interface properties

This section aims to validate the theoretical results of interface properties, Sec 1.7.1. The validation of the results is conducted through both visual inspection of the numerical shape of the interface compared to the derived curves and further verification using the $\int_\Omega(\psi_{grad} + \psi_{bar})dV)$ to numerically compute the integral of interface energy in the simulation, which should be equal to the parameter γ. In numerical simulations, we neglect the density of phase energy ψ_{phas}, as it has no effect on the shape of the interface, only causing the propagation of the ω phase. We have two global unknowns η and $\boldsymbol{u}$, and our domain Ω, which is a line segment of length 10 nm, is divided equidistantly into 5000 parts. Hence, the number of degrees of freedom of the problem is $2 \cdot 5001 = 10002$. The numerical verification of the parameter γ turned out to be very precise for the Landau and double well models, with an error in the double obstacle model caused by the penalty term:

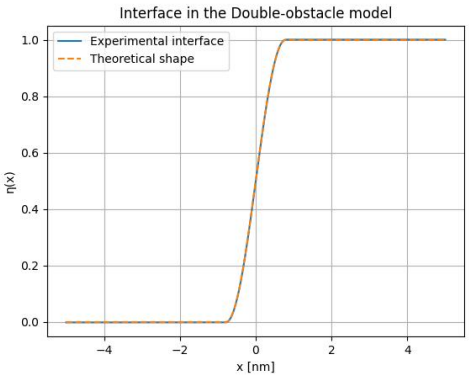

Figure 2.1: Theoretical and experimental shapes of the interface of the double obstacle model.

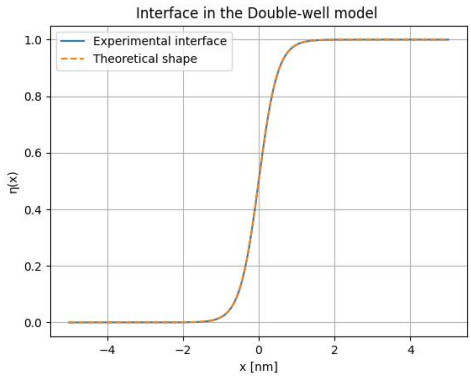

Figure 2.2: Theoretical and experimental shapes of the interface of the double well model.

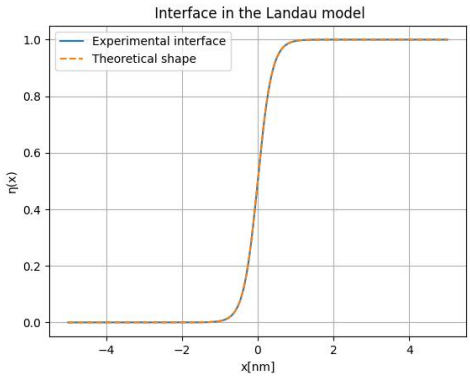

Figure 2.3: Theoretical and experimental shapes of the interface of the Landau model.

$$\begin{aligned}
&\text{Double well:} && \int_\Omega (\psi_{grad} + \psi_{bar})\, dV = (0.2 + 13 \cdot 10^{-8})\ \mathrm{J/m^2}.\\
&\text{Double obstacle:} && \int_\Omega (\psi_{grad} + \psi_{bar})\, dV = 0.1945269\ \mathrm{J/m^2}.\\
&\text{Landau:} && \int_\Omega (\psi_{grad} + \psi_{bar})\, dV = (0.2 + 18 \cdot 10^{-8})\ \mathrm{J/m^2}.
\end{aligned}$$

The shapes of all interfaces perfectly match the theoretical predictions, see Figures 2.1,2.2 and 2.3.

2.2.3 Critical radius of ω phase

The purpose of this subsection is to numerically verify the size of the critical radius, as discussed in Sec. 1.7.2. The theoretical value derived in Sec. 1.7.2 for the critical radius is

$$r = -\frac{\gamma}{\phi} = 1.1834 \text{ nm}. \tag{2.15}$$

We define the numerical radius R as the distance from the center of the phase to the point where the function η reaches the value of 0.5. The value of r can be refined numerically, by including the elastic energy. The elastic energy appears at the interface of the phase ω and can therefore be added, due to its linear dependence on the radius R in simulations, to the interface energy in the following way

$$\gamma_{el} = \frac{\Psi_{el}}{2\pi R} = 0.0026 \text{ J/m}^2, \tag{2.16}$$

where we compute numerically the total elastic energy as $\Psi_{el} = \int_\Omega (\psi_{el}\, dV)$. Then, the critical radius R_{el}, including elastic energy γ_{el}, can be calculated more accurately using the following expression

$$R_{el} = -\frac{\gamma + \gamma_{el}}{\phi} = 1.1988 \text{ nm}. \tag{2.17}$$

Models Landau and double obstacle have the same phase energy difference ϕ, interface energy γ and elastic energy, then these results should be valid for both models.

We solve this problem in a square region with a side length of 20 nm. The region is divided into 300 segments in each direction, and the number of global unknowns is 3, $\boldsymbol{u} = (u_1, u_2)$ and η. The number of degrees of freedom of the problem is $3 \cdot 301^2 = 271803$.

The initial condition is set to $\eta(|\boldsymbol{r}|) = 1$ for $|\boldsymbol{r}| < R_0$ and 0 elsewhere. The values of R_0 are different in order to determine the critical radius. In Figures 2.4 and 2.5, we notice that the numerical radius decreases slightly over time initially (This is caused by the sharp interface of initial condition). Then either rebounds upward or begins to decrease after a period of stagnation, leading us to define the experimental critical radius. The experimental critical radius is defined as the average value between the lowest curve that rebounds upward and the highest curve that begins to decrease, measured at the time when the upper curve reaches its minimum. It is indicated in the caption for Figures 2.4 and 2.5. The experimental radius and the critical radius R_{el}, including elastic energy, coincide in the double obstacle model and its value is $R_D = 1.1988$ nm. In the Landau model, the experimental radius is larger by about one-tenth of a nanometer which corresponds to the $x^* = 0.102$ nm correction and its value is $R_L = 1.295$ nm. On a grid with this resolution, the critical radii can not be determined more precisely.

2.2.4 Rate of the interface

In this section, we verify the fulfillment of the equation for the interface propagation speed, Eq. (1.101) and (1.103). We solve this problem in a square region with a side length of 20 nm such that domain was $|x| < 10$ nm and $|y| < 10$ nm. The region is divided into 200 segments in each direction, and the number of global unknowns is 3, $\boldsymbol{u} = (u_1, u_2)$ and η. The number of degrees of freedom of the problem is 121203 in all cases. We set initial condition $\eta(x, y) = 1$ if $y > 9\text{nm} - x$, and 0 elsewhere, in corner situation and $\eta(\boldsymbol{r}) = 1$ if $|r| < 1.5$ nm, and 0 elsewhere, in circle situation.

In the corner situation, both models were delayed compared to the theoretical solution in their distance from the corner. The ω phase filled the space in the

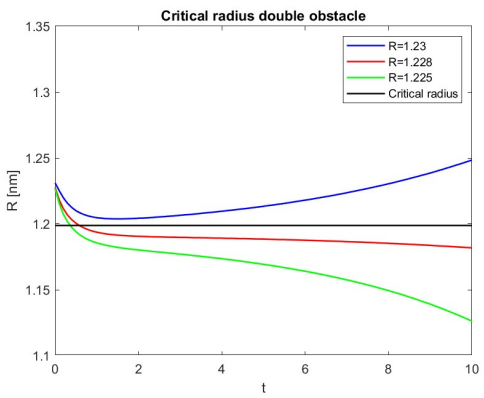

Figure 2.4: Dependency of the numerical radius on time in double obstacle model. The blue curve represents the lowest curve that rebounds upward, while the red curve represents the highest curve that begins to decrease. The average between them at time 1.9 (black line) corresponds to the experimental critical radius, which coincides with R_{el}, hence referred to as the Critical radius.

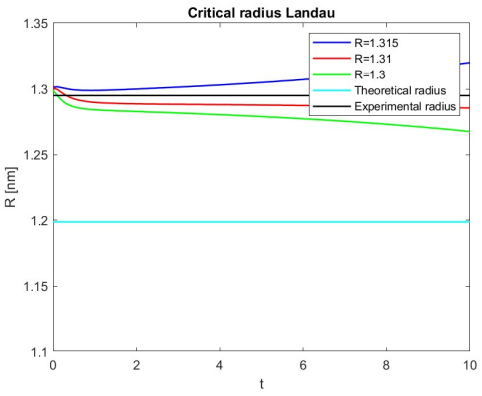

Figure 2.5: Dependency of the numerical radius (the distance from the phase center to the point where the function η reaches 0.5) on time in Landau model. The critical radius R_{el} is represented by the turquoise line, while the experimental critical radius is black line and it is equal to 1.295 nm. The difference between them is 0.096 nm which corresponds to the $x^* = 0.102$ nm correction.

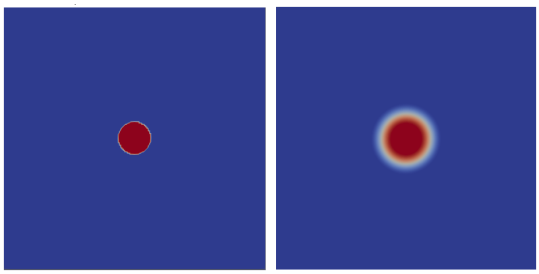

Figure 2.6: The evolution of the phase ω in the double obstacle model. The initial condition is $\eta(|r|) = 1$ for $|r| < 1.23$ nm, and 0 elsewhere. The evolution in the right image shows its increase at $t = 22$, with a numerical radius equal to 1.52 nm.

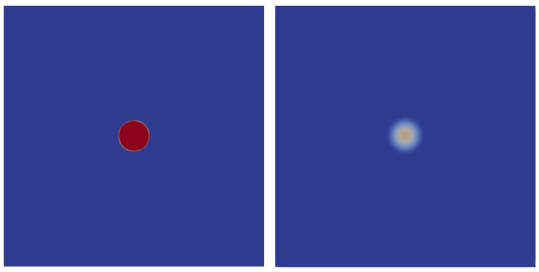

Figure 2.7: Evolution of the double obstacle model with the initial condition $\eta(|r|) = 1$ for $|r| < 1.22$ nm, and 0 elsewhere, on the right side. On the left side, we observe a decrease in the phase at $t = 15$ with a numerical radius equal to 0.8 nm.

double obstacle model 2.21 time units later, and in the Landau model 4.43 time units later than the theoretical prediction, see Fig. 2.8. This situation does not entirely correspond to the theoretical scenario because the phase interface is not perfectly straight but bends at the boundary regions, as illustrated in Fig. 2.10. Consequently, the experimental values do not completely align with the theoretical results.

In the circular situation, the double obstacle model evolved almost identically to the theoretical prediction, with the radius differing by 0.096 nm at the final time of 30. The Landau model, on the other hand, differed by 1.02 nm at the final time which corresponds to the corrected equation (1.105) , see Fig. 2.9 and

2.11 .

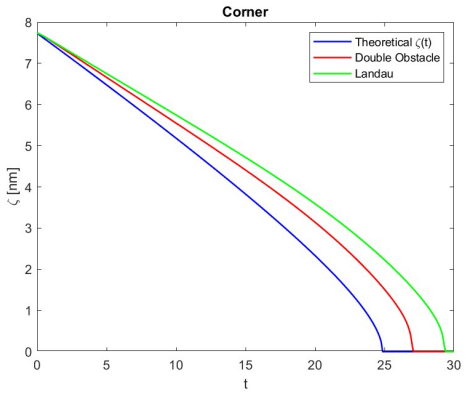

Figure 2.8: The evolution of the distance from the lower left corner to the interface (the interface is taken where $\eta = 1/2$), denoted as the variable $\zeta(t)$. Both models are delayed due to bends on the boundary.

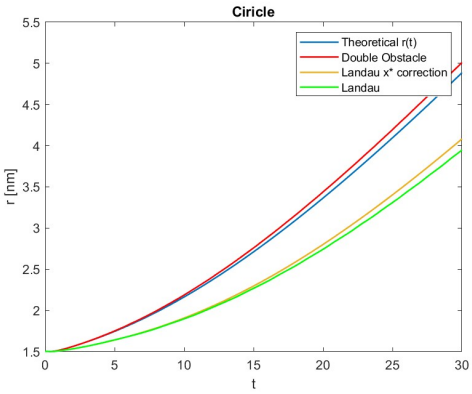

Figure 2.9: The evolution of the distance from the center of the circle to the center of the interface denoted as $r(t)$. The double obstacle model corresponds to the theoretical equation and Landau model to the corrected equation.

Figure 2.10: The evolution of the Landau model interface in a corner situation. The Figures are taken at times $t_1 = 0$, $t_2 = 7$, $t_3 = 15$, and $t_4 = 28$, corresponding to distances $\zeta_1 = 7.73$, $\zeta_2 = 6.53$, $\zeta_3 = 4.83$, and $\zeta_4 = 1.35$ nanometers, respectively.

2.3 Two ω variants

2.3.1 Interface energy and filled volume of transformation

In this section, we focus on simulation of two ω phases. Our computational domain is square, with the same dimensions and grid density as in Subsec. 2.2.4, but we have two phase field variables, thus the number of degrees of freedom is 161604. The initial conditions were set as follows: $\eta_1(x, y) = 1$ if $(x + 5\text{nm})^2 + (y + 5\text{nm})^2 < 4.5^2\text{nm}$, otherwise 0, and $\eta_2(x, y) = 1$ if $(x - 5\text{nm})^2 + (y - 5\text{nm})^2 < 4.5^2\text{nm}$, otherwise 0. It is two circles with a radius of 4.5 nm, the first centered at $(-5\text{nm}, -5\text{nm})$ and the second at $(5\text{nm}, 5\text{nm})$, see Fig. 2.14 in time $t = 0$. We define $V = 400\text{nm}^2$ as the total volume of the domain, $V_D(t)$ and $V_L(t)$ as the volumes filled by both ω phases at time t in the double obstacle and Landau models, respectively. The final volumes are denoted as $V_D^* = V_D(100)$,

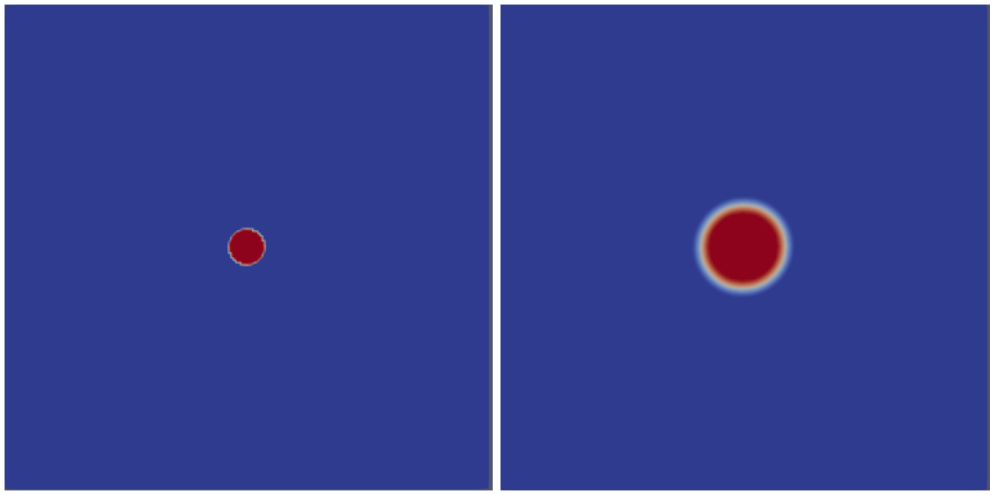

Figure 2.11: The phase propagation evolution in the double obstacle model. The images are captured at times $t_1 = 0$ and $t_2 = 15$, with corresponding radii $r_1 = 1.5$ and $r_2 = 2.74$ nanometers, respectively.

$V_L^* = V_L(100)$. If we speak generally about both models together, then $V_\omega(t)$ represents the filled volume by ω phases and V^* their final volume.

The Landau model propagated slower than the double obstacle model, as evident from the Figure depicting the ratio of the volume of both ω phases to the total volume with respect to time, Fig. 2.12. Moreover, the ω phase filled only $0.97 = V_L^*/V$ of the space in the Landau model. In double obstacle all ω phases filled the space $1 = V_D^*/V$.

In order to compare the interface energies of both models, it is reasonable (due to their slightly different propagation speed) to plot their energy with respect to $V_\omega(t)/V^*$ (then they are in the same phase of evolution), see Fig.2.13.

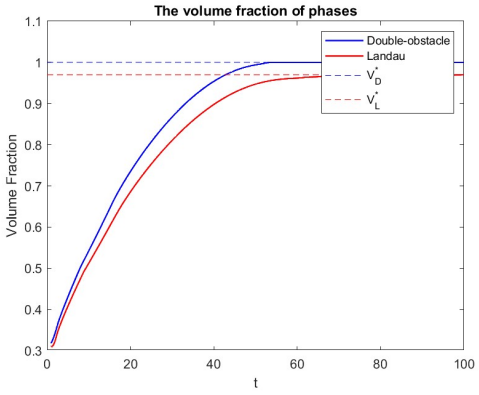

Figure 2.12: Evolution of the volume fraction of ω phases $V_D(t)/V$ and $V_L(t)/V$. The dashed lines indicate the final volume fractions. It is evident that the ω phases in the Landau model do not fill the entire domain, whereas in the double obstacle model they do.

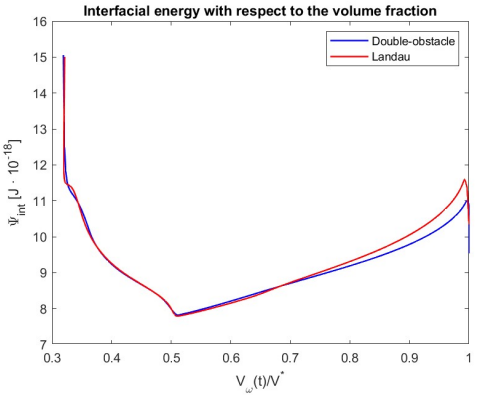

Figure 2.13: Interface energy with respect to their normalized volume fractions, i.e., $V_D(t)/V_D^*$ and $V_L(t)/V_L^*$ (where both fractions reach 1 in the end). In fact, it is a parametric curve $(V(t)/V^*, \Psi_{int}(t))$. The interface energy in Landau model is grater.

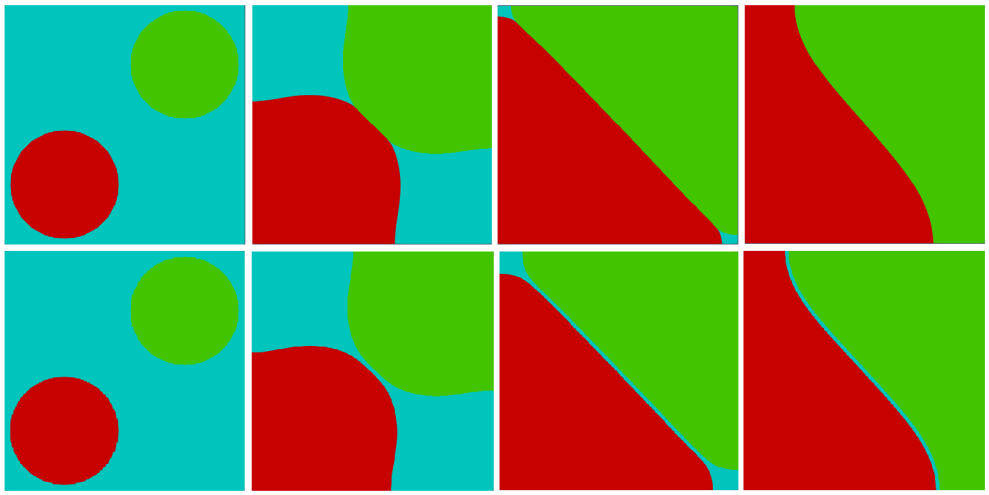

Figure 2.14: The upper set of Figures is captured from simulations using the double obstacle model, while the lower set corresponds to the Landau model. The Figures are taken at times $t_1 = 0$, $t_2 = 17$, $t_3 = 50$, $t_4 = 100$. It can be observed that the Landau model evolves slightly slower. Moreover, it is evident that in the Landau model, the ω phases do not touch, while in the double obstacle model they do.

2.3.2 Testing of material parameters

As mentioned, it is experimentally observed that the ω phase does not entirely fill the volume of the body. In the previous section, we demonstrated that with material parameters set according to Table 2.2.1, the Landau model manage to avoid completely filling the space, while the double obstacle model fill the space. In this section, we adjust the material parameters of the double obstacle model in order to achieve non-filling of the space by ω phases.

Our domain is a square such that $|x| < 10$ nm and $|y| < 10$ nm. The region is divided into 200 segments in each direction, and the number of global unknowns is 4, $\boldsymbol{u} = (u_1, u_2)$ and η_1, η_2. The number of degrees of freedom of the problem is 161604 in all cases. The initial conditions is set as follows: $\eta_1(x, y) = 1$ if $(x + 5\text{nm})^2 + (y)^2 < 4^2\text{nm}$, otherwise 0, and $\eta_2(x, y) = 1$ if $(x - 5\text{nm})^2 + (y)^2 < 4^2\text{nm}$, otherwise 0. It is two circles with a radius of 4 nm, the first centered at $(-5\text{nm}, 0\text{nm})$ and the second at $(5\text{nm}, 0\text{nm})$. Total volume of domain is $V = 400$ nm^2, V^* denotes the volume filled by ω phase in stationary converged states.

The material parameters is set as $\ell_{\beta\omega} = 1$ nm, $\ell_{\omega\omega} = 0.2$ nm, $\gamma_{\beta\omega} = 0.2$ J/m^2, $\gamma_{\omega\omega} = 0.8$ J/m^2 in the firs situation. The β phase is present here, but always in combination with the ω phase, so its volume fraction is never equal to 1. The ω phase filled $V^*/V = 0.973$ of the total volume.

The material parameters is set as $\ell_{\omega\omega} = 0.5$ nm, $\ell_{\beta\omega} = 1$ nm, $\gamma_{\omega\omega} = 0.2$ J/m^2, $\gamma_{\beta\omega} = 0.8$ J/m^2 in the second situation. The β phase appeared alone amidst the ω phases, so its volume fraction is locally equal to 1. The ω phase filled $V^*/V = 0.96$ of the total volume, which is similar to the firs case. So the β phase is more concentrated, but on a narrower interface.

The material parameters is set as $\ell_{\beta\omega} = 2$ nm, $\ell_{\omega\omega} = 0.5$ nm, $\gamma_{\beta\omega} = 0.2$J/m^2, $\gamma_{\omega\omega} = 3$ J/m^2 in the third situation. The β phase appear alone and the ω phase filled only $V^*/V = 0.906$ of the total volume.

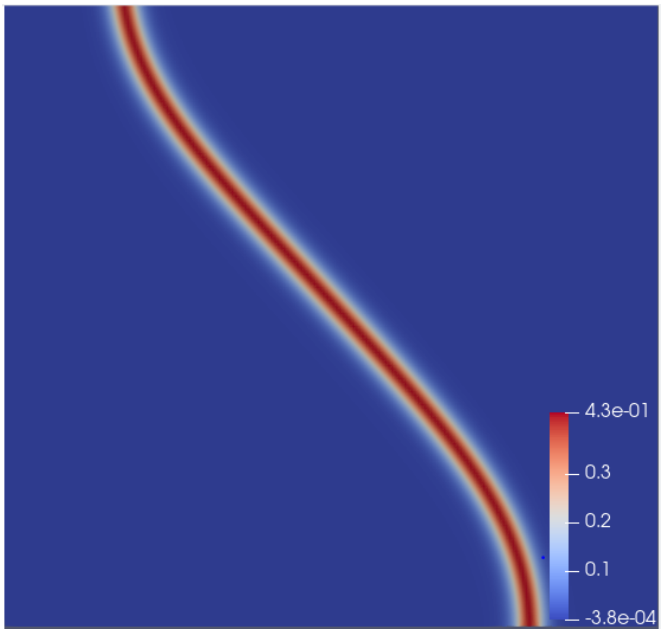

Figure 2.15: The remaining β phase in the Landau model, calculated as $1-\eta_1-\eta_2$, from $t = 100$.

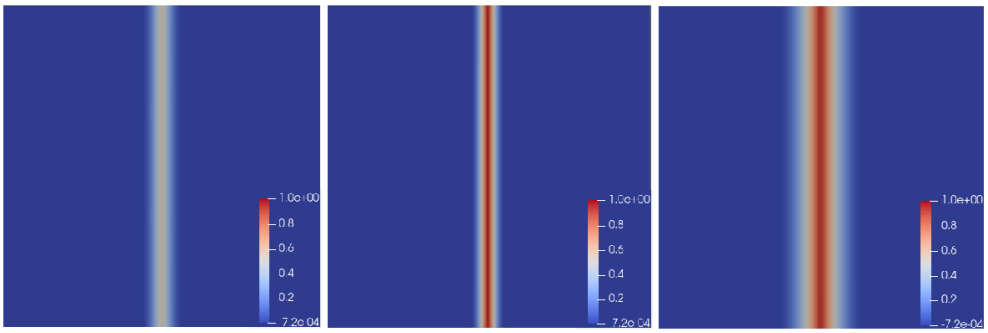

Figure 2.16: The remaining β phase in the double obstacle model, calculated as $1-\eta_1-\eta_2$, from stationary converged states. The first described situation is on the left Figure, the second one in the middle, and the third on the right.

2.4 Four ω variants in 3D

In this section, we present the results of simulation in 3D. We randomly distributed 16 phase grains from each of the four ω variants with a radius of 3 nm into a cube with a side length of 60 nm (total number of grains is 64). The cube is divided into 128^3 segments in each direction, with seven global unknowns ($\boldsymbol{u}$, η_1, η_2 η_3, η_4), thus the total number of degrees of freedom is 15 026 823. This very large problem was computed at the Snehurka cluster using 216 cores. As before, the non-linearities are trested with the Newton solver, but istead of using the direct linear solver, we employe iterative GMRES solver with geometric multigrid as a preconditioner[1] (V-cycle with 4 levels, smoother GMRES with point-block Jacobi as its preconditioner, coarsest level direct solver MUMPS).

[1]With the help of the supervisor.

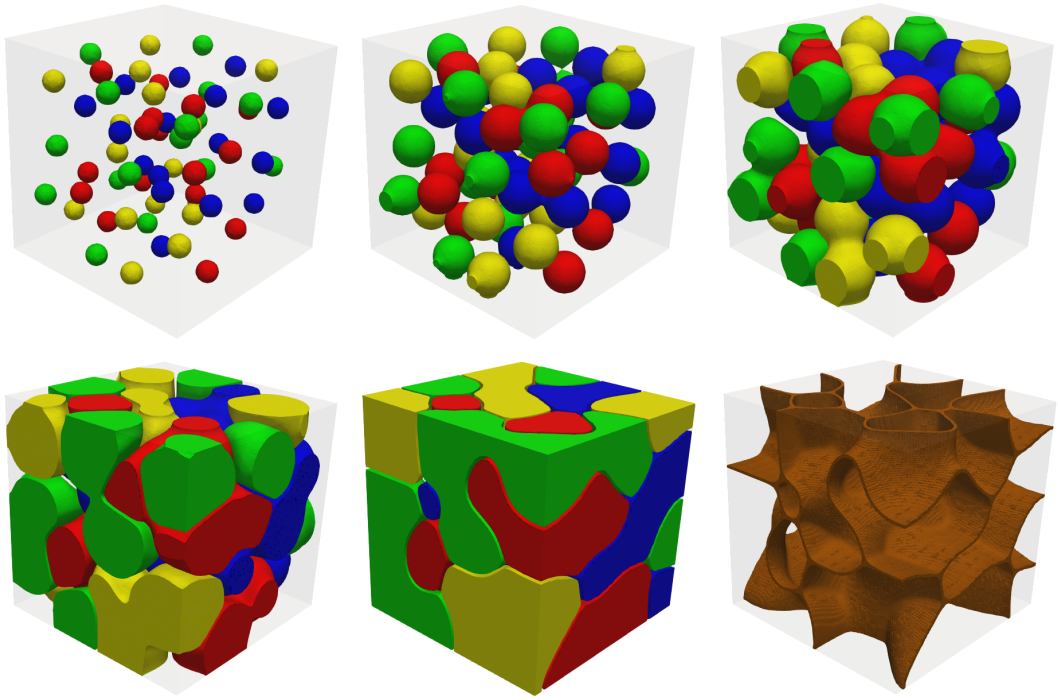

Figure 2.17: Evolution of ω phases. The first five Figures are taken in time $t = 0$, $t = 13.7$, $t = 19.5$, $t = 29.5$, $t = 53.9$ respectively. The last Figure shows remaining β phase from stationary converged state $t = 53.9$.

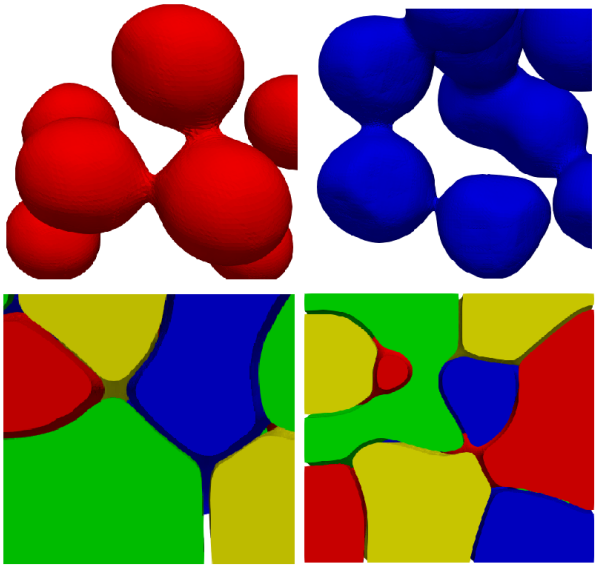

Figure 2.18: The upper figures shows the merging of two identical variants of the ω phases, lower figures shows free space between different variants of ω.

We employ the double obstacle potential with the following parameters: $\ell_{\omega\omega} = 0.5$ nm, $\ell_{\beta\omega} = 1$ nm, $\gamma_{\omega\omega} = 0.2$ J/m^2, $\gamma_{\beta\omega} = 0.8$ J/m^2.

Conclusion

Theoretical part

In the first chapter, we described the basic of modeling the β to ω transformation. We described the three existing models: Landau, double obstacle, and double well, for phase transformations. We discussed the double well model only for a single phase transition and calculated its interface properties. Furthermore, we focused on describing multiple phase-field variables using the double obstacle and Landau models and compared their properties. In the double obstacle model, we derived a more suitable form of the interface energy for numerical implementation and deduced its qualitative properties, such as interface energy, minimum grain size, and interface propagation velocity. In the Landau model, we were able to separate the chemical energy into phase energy and barrier energy. Due to this separation, we were able to appropriately represent material parameters so that the interface energy γ had the same significance as in the previous two models, the parameter ϕ represented the energy difference between phases, and the parameter δ determined the width of the interface. The main difference between the Landau model and the previous models is the non-linear mixing in phase energy, which shifts the phase energy towards the ω phase. This non-linearity necessitated a correction in the theoretical calculations, as we must subtract x^* from the radii for calculating phase energy. The relationship between the parameter δ and the parameter ℓ was set so that the interface would propagate at the same speed. However, we suspect that due to the mentioned non-linearity, this result is valid only for planar interfaces. If the interface is convex, the Landau model lags behind, and if it is concave, the Landau model should outperform the double obstacle model. In the first chapter, we were ultimately able to derive theoretical properties even for the Landau model with this correction.

Numerical implementation

In the numerical part, we firstly described the numerical scheme and verified the analytical benchmarks. All interface shapes matched perfectly with the theoretical ones. The interface energy in the double well and Landau models came out precisely, while in the double obstacle model, its numerical value is influenced by the penalty. The derived critical radii in the double obstacle and Landau models (after correction due to phase energy) came out accurate to hundredths of a nanometer. The interface propagation speed in the circular case matched the theoretical prediction (again after correction in the Landau model). In the corner situation, the theoretical prediction differed from the numerical simulations, and we suspect that it is due to the curvature of the interface at the boundary of the domain. In the next section, we compared the evolution of two phases in the Landau and double obstacle models. The parameters were set to qualitatively match the models. The ω phase did not fill the space in the Landau model, while it did in the double obstacle model. The interface energy corresponding to the volume fraction also matched. In the following section, we showed that by increasing the parameter $\gamma_{\omega\omega}$ (interface energy between ω phases), it is also possible in the double obstacle model to prevent the ω phase from filling the space. In

conclusion, the models qualitatively corresponded to each other.

Possible improvements

The non-elastic part of energy of the Landau model is determined in the case of multiple phases by only three parameters, so it is not possible to vary other energies and widths of interfaces between β and ω, and between ω and ω interfaces. It would be useful to generalize this model. Another possible improvement is to analytically or numerically solve the stationary state of the interface between two ω phases similarly to how it is done in this thesis for the interface between β and ω phases.

Bibliography

[1] J. Šmilauerová. Phase transformations in modern titanium alloys. *Charles University in Prague, PhD thesis*, 2016.

[2] K. Bhattacharya. *Microstructure of martensite: why it forms and how it gives rise to the shape-memory effect.* Oxford University Press, 2003.

[3] B. Tang. A phase-field approach to athermal $\beta \rightarrow \omega$ transformation. *Computational materials science 53.1*, pages 187–193, 2012.

[4] T. Lookman H. K. Yeddu. Phase-field modeling of the beta to omega phase transformation in zr–nb alloys. *Materials Science Engineering A*, pages 46–54, 2015.

[5] A. Saxena M. Sanati. Landau theory of domain walls for one-dimensional asymmetric potentials. *American journal of physics*, pages 1005–1012, 2003.

[6] J. Hron P.E. Farrell S. Stupkiewicz K. Tůma, M. Rezaee-Hajidehi. Phase-field modeling of multivariant martensitic transformation at finite-strain: computational aspects and large-scale finite-element simulations. *Comput. Meth. Appl. Mech. Eng.*, (377:113705), 2021.

[7] I. Steinbach. Phase-field models in materials science. *Modelling Simul. Mater. Sci. Eng.*, 2009.

[8] J. W. Cahn S. M. Allen, T. Lookman. A microscopic theory for antiphase boundary motion and its application to antiphase domain coarsening. *Acta Metalurgica*, 27:1087–1095, 1978.

[9] K. Sejková. Application of the spectral method to the simulation of the phase-field model for martensitic transformation. *Charles University in Prague, Master thesis*, 2020.

List of Figures

List of Tables